Aus der Pferdeklinik
der Vetsuisse-Fakultät Universität Zürich
(Direktor: Prof. J. A. Auer)

und

aus dem AO-Forschungsinstitut Davos
(Direktor: Prof. E. Schneider)

Arbeit unter der Leitung von
Dr. R. G. Richards
Bio-Performance of Materials & Devices

In vivo biocompatibility study of different calcium-phosphate surfaces for implant bone integration

Inaugural-Dissertation
zur Erlangung der Doktorwürde
der Vetsuisse-Fakultät Universität Zürich

vorgelegt von

Patrick Schlegel

Tierarzt von

Buchs-SG (CH)

Genehmigt auf Antrag von

Prof. Dr. J. A. Auer, Referent
Prof. Dr. E. Schneider, Korreferent

Davos
2004

Contents

Summary

Implant loosening is an unresolved complication associated with internal fixation. It is generally accepted that this problem may be overcome by modifying the implant/bone interface for improved osseous integration. Improved osseous integration may be obtained by the use of hydroxyapatite (HA) or tricalcium phosphate coatings. Unfortunately, these coatings have been limited by their low strength of adhesion to the implant surface or in cohesion within their layers. Anodic Plasma-chemical (APC) treatment has been developed to incorporate electrolytes into the surface to produce various microtopographies and chemistries. The idea developed was to bind calcium and phosphate to the metal surface to produce superior adhesive strength of the coating and an osseoconductive surface. The hypothesis is that this new surface treatment with APC (shown to adhere with 4 times strength of HA to a titanium surface, Frauchiger 2002), will be able to overcome the deficiencies observed with HA. Therefore, the biocompatibility and osseoconductivity of APC surfaces was compared to standard HA coated and non-coated titanium (Ti) implant screws as controls.

Cortex screws were implanted into the craniomedial cortex of adult female Swiss alpine sheep tibiae. One each of the following of 4.5mm titanium screws, either calcium phosphate coated, deposited using anodic plasma-chemical treatment (APC-CaP), or phosphoric acid coated, deposited by APC treatment (APC-P), hydroxyapatite-coated (plasma sprayed and chemically deposited), or uncoated but anodised commercially pure titanium screws were implanted on the left and right tibia of each sheep. The location of each individual screw type was varied in each sheep, so that each screw had been placed once in each location of the template. The observation time was 12 weeks. Radiography images of the implantation site for monitoring the thickness of the cortex on each screw surface and for possible signs of radiolucency were taken at two-week intervals starting on the day of surgery. To estimate implant anchorage, induced by the different surface types, the screw insertion and extraction torques were measured initially and after sacrifice at 12 weeks.

As a tendency, the increase of the cortex thickness with time was faster for APC-coated screws (CaP and P) than for the HA- coated screws (between week 4-6) indicating an accelerated early bone healing. After 12 weeks the thickness of the cortex of the screw type coated in calcium phosphate (APC-CaP) at the lower current was significantly higher than

that of the HA-coated screws. The difference between cortex thickness of the screw type coated with APC-CaP at higher current and the HA-coated screws was not significant.

Screw insertion torques did not significantly differ between the various types. The screw types coated with HA (plasma sprayed and chemically deposited) exhibited significantly higher removal torques than all other surfaces. The 4 surfaces coated with the APC method exhibited significantly higher removal torques than the uncoated anodised CpTi surface. These differences may be attributed to variation between the types of coating thickness, varying from zero on the uncoated CpTi, to a few micrometers with the APC surfaces to 60 to 80 μm with the HA coatings. This increase will produce a pre-load on the screws giving a tighter fit of the implant in the bone, which is known to increase osseointegration and therefore increase the amount of torque required for extraction. To produce screws with these various coatings with only a 1-2μm in diameter difference would require to firstly produce the base screw with only 1-2μm tolerance and vary by the thickness of the applied coating, which is currently technically not possible (current screw tolerances are between 0.05-0.08 mm).

A qualitative histomorphological assessment of the tissue adjacent to the screws was completed following histological preparation after sacrifice at 12 weeks. Bone apposition onto the various screw surfaces was measured using bright field light and fluorescence microscopy. No significant difference among the tested screw types was observed in the area of remodelling of the original bone, as well as in the area of the new bone formation towards the screw tips on the endosteal side. Nevertheless, the APC-CaP screws (both current densities) were found to have more implant/calcified bone contact than the other surfaces. Encapsulation of the implant with fibrous tissue was not observed with any screw type tested. Similar results were found for the new bone formation region (towards the tip the screw in the medullary canal).

The APC-CaP proved to be biocompatible for bone formation and remodelling. Regarding bone growth induction and the apposition onto the implant surface, the APC coatings behaved as well as commercial HA coatings. The unloaded model used here with the screws does not appear to be sensitive enough to show differences that may occur in more testing clinical situations with coatings on other types of implants, in other anatomical locations.

1. Introduction

The surface properties of an orthopaedic implant material are of fundamental importance for the clinical success of the device. The consistency of the implant-bone interface contributes to the success of the implant (Branemark *et al*., 1977). Knowledge and assessment of the microtopography and micro-chemical characteristics of the surface are needed to understand the interactions at the interface of the tissue and implant, which finally represent the key to a successful integration of the implant into the body. For permanent implants, such as prostheses for joint replacements, spinal cages for spine fusion or dental implants, it is essential that the surrounding bony tissue integrates well (osseointegration) and the surface of the implant favours the process of cell attachment, adhesion and spreading (Bagambisa *et al*., 1990). Osseointegration is the direct contact at the light microscope (LM) level (micrometer range) between living bone and an implant without a soft-tissue interface (Albrektsson *et al*., 1981; Albrektsson and Johansson 2001) and is essential for stable implant anchorage (Branemark *et al*., 1977). Dental titanium structures with a microstructure of a few microns average roughness are known to provide a good and large contact area for osseointegration (Buser, *et al*., 1991) and this is likely to also be the case for orthopaedic implants. Although the clinical term osseointegration describes the anchorage of endosseous implants to withstand functional loading, it provides no insight into the mechanisms of bony healing around such implants (Davies, 1998). An understanding of the progression of bone healing events around endosseous implants is critical for developing functional implant surfaces.

Hypothesis of bone remodelling next to an implant.

Endosseous integration: Whenever an implant is brought in contact with bone, blood proteins are adsorbed onto the surface of the implant (Gemmell and Park, 2000). Though other proteins attach first, eventually mostly fibrin is found, which contacts both the bone and implant. Along these fibrin fibres osteogenic cells from the marrow and the endosteum, migrate towards the implant and during this migration differentiate into mature osteoblasts. Osborn and Newesley (1980) hypothesised that two processes of endosseus healing occur, namely distance osseogenesis (Figure 1.1) and contact osseogenesis (Figure 1.2)

During distance osseogenesis the bone surface grows toward the implant, similar to normal appositional bone growth, with the existing bone providing the osteogenic cells that lay down new matrix. Therefore bone does not form on the implant itself but grows towards and to

surround an implant. In this case it is thought not possible to attain bone bonding because the bone surrounds the implant rather than bonding directly to it and the interface of connective tissue extracellular matrix (ECM) is unstable.

During contact osseogenesis the implant surface is colonised by a population of osteogenic cells through migration before the cells stop migrating and start bone matrix formation. Therefore bone grows directly on the implant surface which can then fuse with native bone thus forming a stable connection. During loading, movement from the implant should not happen since bone bonds directly to the implant surface.

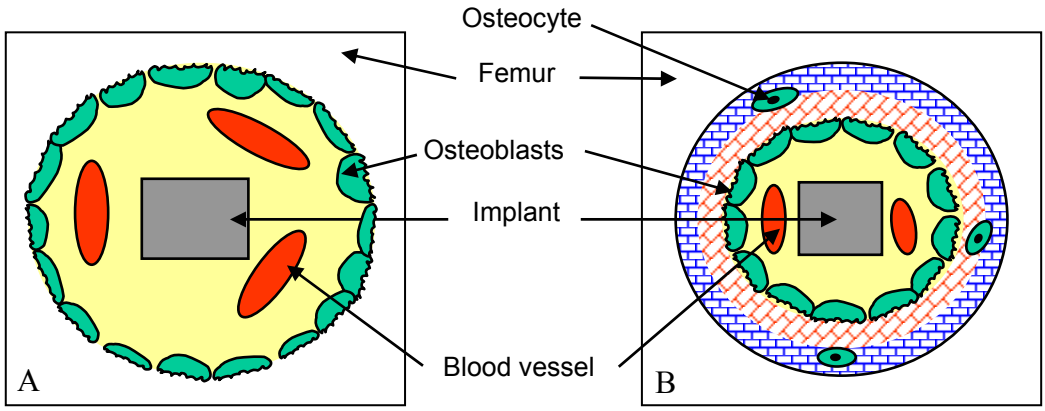

Figure 1.1 Diagram of distance osseogenesis. A) Osteogenic cells line the original bone surface, the blood supply being between the cells and implant. B) bone is laid down on the original bone surface. Modified from Davies, 1998.

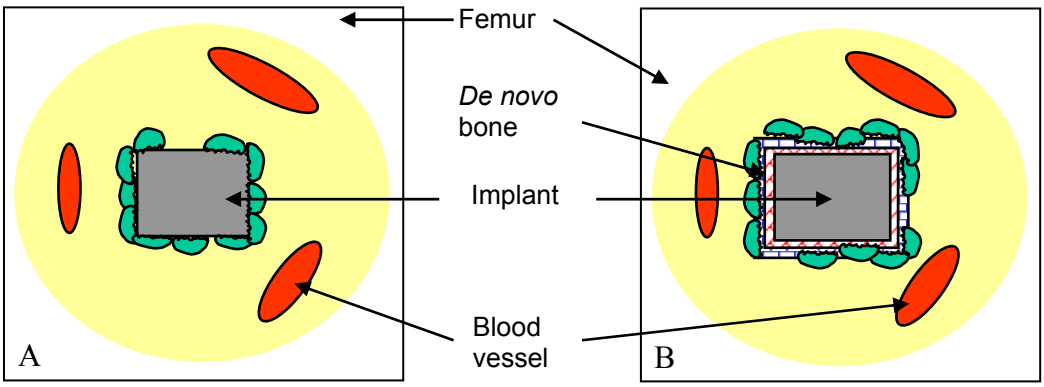

Figure 1.2 Diagram of contact osseogenesis. A) Osteogenic cells have been recruited to the implant surface, the blood supply being between the cells and original bone. B) *De novo* bone is laid down on the implant surface .Modified from Davies, 1998.

De novo bone formation on implant surfaces and natural bone remodelling sites has been confirmed by *in vitro* and *in vivo* experiments to be processes that are quite different to fracture healing. Fracture healing is divided into 3 phases. First an inflammatory response where the fractured bone is immobilised and repair cells are activated. After around 1 month,

periosteal and medullary calluses (fibrocartilage) are created by osteoblasts from the periosteum and marrow and these interim calluses become calcified. Once the callus structure is as rigid as bone, a bony union has been achieved. Repaired broken bones are as strong as intact original bone but of greater mass (accordingly less mechanically efficient). Modelling and remodelling restores the original site form and bone internal structure.

De novo bone formation is a cascade with four steps. At first differentiating osteogenic cells secrete a collagen-free organic matrix, providing nucleation sites for calcium phosphate mineralisation. The matrix is composed of non-collagenous bone proteins, such as osteopontin and bone sialoprotein (Shen *et al*., (1993). These proteins provide nucleation sites where crystals of calcium phosphate grow. Upon this collagen is deposited which subsequently mineralises. Therefore, the collagen section is separated from the substratum by a collagen-free calcified tissue layer. This layer is approximately 0.5 μm thick, as are cement lines that form the interface between old and new bone at remodelling sites. This may provide an explanation for the evidence of accelerated early bone healing around calcium phosphate – based implant surfaces (Moroni *et al.*, 1994, Hanawa *et al.,* 1997). Bone bonding is thought of as a chemical interaction where collagen from the bony compartment interdigitates with the surface of the implant. However, in the case of *de novo* bone this is implausible since the implant surface is thought of as collagen free. Bonding can only be achieved by micromechanical interdigitation of the cement line with the material surface.

During distance osseogenesis osteoblasts secrete bone matrix on existing bone so cells are pushed towards the implant. This results in enclosed osteoblasts, which cut off from blood supply, die. In contact osseogenesis the osteoblast comes into direct contact with the surface, which is dependant upon fibrin anchorage onto the implant. The surface topography and chemistry determine the migration of the osteoblasts onto the implant surface. If the implant surface is smooth, adsorbed fibrin will detach from the implant during wound healing contraction, and even during the actual process of the migration of the osteogenic cells through the fibrin matrix, due to lack of anchorage to the substrate (Figure 1.3). Consequently the migrated osteogenic cells and the secreted matrix will not be in contact with the implant surface. If the implant surface has the correct microroughness, fibrin anchorage survives contraction from wound healing. The migratory pathway of the differentiating osteogenic cells is sustained allowing the cells to reach the implant surface before stopping migrating and secreting bone matrix (Figure 1.4). Therefore the structure of the implant surface is essential for an optimal implant bone anchorage with regard to the attachment of fibrin.

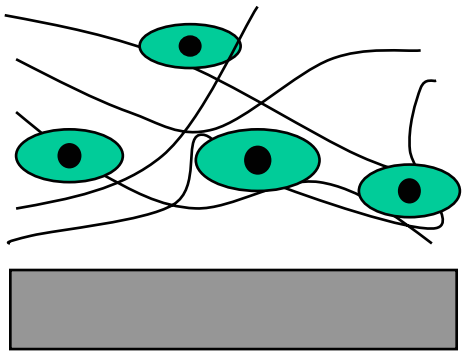

Figure 1.3 A smooth surface affects fibrin attachment during wound contraction. From Davies, 1998

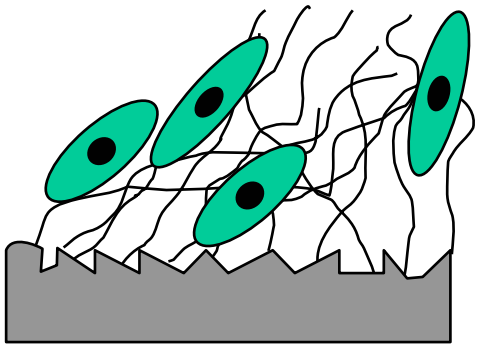

Figure 1.4 A rough surface affects fibrin attachment during wound contraction. From Davies, 1998

Contact osseogenesis can be initiated by providing a rough surface for fibrin anchorage, fibrin adsorption being higher on rough material in comparison to smooth material (Nygren *et al*., 1997). Once the bone has a stable connection to the implant, native bone movement may occur between bone and implant if there is low friction between them. Encouraging osteogenic cell migration along the implant surface and ensuing mineralisation is the next step for increasing bone/implant friction. Moreover the microtopography could be used to accelerate mineralised matrix production upon the implant surface. In this current study several microrough calcium phosphate –based surfaces were investigated to see if they increased boney integration or accelerate early bone healing around them.

Hydroxyapatite (HA) and other calcium phosphate (Ca-P) coatings (which also have micro-rough surfaces) are known to favour osseointegration around stainless steel and titanium implants because of their close chemical structure to mineralised bone. These coatings have been shown to promote osseointegration by stimulating bone growth onto the surface (Ducheyne and Qiu Q 1999). External fracture fixator pins coated by plasma spraying with HA have been tested in a long term, unloaded, ovine model (Moroni *et al.*, 1996), showing a reduction in the incidence of pin loosening by improved osseointegration of the HA coated pins compared to uncoated pins. A clinical trial confirmed these results (Pomer *et al.,* 2002). Nevertheless, problems still exist with the current HA and Ca-P coatings. They are usually produced ~10-100µm thick and can fail during long-term use, in either adhesion (delamination) to the implant itself or in internal cohesion of the actual coating (Rokkum *et al.,* 2003). The clinical study by Pommer *et al.* (2002) also found HA delamination on pin removal. If this happens *in situ* it may encourage fibrous tissue formation at the implant surface and could result in implant loosening.

This along with production costs has induced the search for a coating that encourages good fibrin attachment and boney integration, while being good for adhesion to the implant surface and cohesion within its internal structure. It is difficult to produce a uniform Ca-P coating on implants with complex three-dimensional structures such as is found with screw threads or spinal cage implants and a coating which could accomplish this would be beneficial. With current techniques plasma spray coating can not be produced less than 30-40μm thick.

Commercially pure titanium (CpTi) readily forms a compact oxide layer, which stabilises the more reactive metal underneath, separating it from the electrolytic body fluids. The thickness of the oxide formed depends on the oxidation procedure applied (spontaneous formation, electrochemical anodisation, thermal oxidation, etc.) and is normally thinner than 0.2 μm. Spontaneously formed oxide layers are amorphous. Specific treatments can lead to thicker surface layers with different crystalline structures. The degree of crystallinity increases with the thickness of the oxide, the thickness increases with increasing formation voltages in anodic oxides and with increasing temperatures in thermal oxides (Lausmaa, 1991). The oxide layer may be damaged by abrasion, but re-oxidization occurs nearly immediately (Witt *et al*., 1991). Anodic spark discharge (ASD) can break down this oxide by discharging sparks at high voltage to produce a thin microrough and microporous amorphous titanium oxide containing calcium and phosphate (Kurze *et al*., 1986; Ishizawa and Oginio, 1995; Ishizawa *et al*.,1995; Ishizawa *et al*.,1997). Surfaces produced by this method with a thickness of about 5 μm, have been tested for biocompatibility *in vitro* with cytotoxicity tests and *in vivo* for osseointegration (Fini *et al*., 1999). Biocompatibility has been defined (Williams, 1987) as "the ability of a material to perform with an appropriate host response in a given application" explaining its biological and functional aspect.

Neither infection nor the presence of inflammatory cells was observed in the *in vivo* study and osseous bridges were observed between the cancellous bone and the implants (Fini *et al*., 1999). The ASD surfaces tested had the lowest bone apposition, which the authors attributed to degradation of the amorphous oxide film. Unfortunately the authors did not consider measuring the implant to bone bonding strength, which they realised, was important, since enhanced bone apposition alone does not necessarily imply greater bone bonding strengths (Chae *et al*., 1992).

Anodic plasma-chemical (APC) treatment, where ASD is performed in the presence of electrolytes, also breaks down this naturally occurring oxide film on titanium as part of the process to form an inorganic glass-ceramic-like coating as a final product (Schreckenbach *et al*, 1999). APC treatment has a much better adhesion strength (60 MPa) compared to standard HA-implant adhesion (ISO 13779-2, HA 15 MPa, Frauchiger, thesis 2002).

The *in vitro* cytocompatibility results of these APC surfaces have shown positive results in terms of fibroblast and osteoblast adhesion and spreading (Baxter *et al.,* 2001) (cytocompatibility is one aspect of biocompatibility; the cellular response to a biomaterial, Richards *et al*, 2001). The question in this present study is whether APC treatment can produce optimal micro-topography and micro-chemistry characteristics for bony integration and bonding strength for implants used in fracture fixation compared to currently manufactured titanium and HA coated implants such as VPS (hydroxyapatite-plasma coating) HA representing a thermally sprayed coating and Bmim (biomimetic) HA which represents a chemically deposited soluble hydroxyapatite coating.

The controls of VPS and Bmim were used as standard surface modifications. Plasma sprayed HA coatings are a standard method of titanium surface modification. HA powder is injected into an inert gas plasma jet, exposed shortly to a very high temperature of over 15'000 °C usually under vacuum, which cause the particle surfaces to melt and deposit on the cooler titanium in a partly armorphous form (Gruner 2001) forming a coating (thickness 30-250µm). Thinner coatings have more strength and thicker ones more resistance to dissolution / resorption. Chemically prepared HA coating, by soaking titanium in NaOH at 60 °C forms a titanium hydrogel on the surface. Heat treatment at 600 °C densifies the gel resulting in an armorphous sodium titanate layer. When soaked in simulated body fluid, the alkali ions dissolve, the titanate transforms into a hydrogel inducing nucleation of apatite forming a 5-10µm HA layer (Kim *et al.,* 1999).

1.1 Anodic plasma chemical (APC) treatment of screws

Production of the four APC surfaces (by Vinzenz Frauchiger, LSST, ETH Zürich) involved using a titanium screw as an anode immersed in a conductive electrolytic solution containing ions desired in the final surface layer. The equipment set up is depicted in figure 1.5.

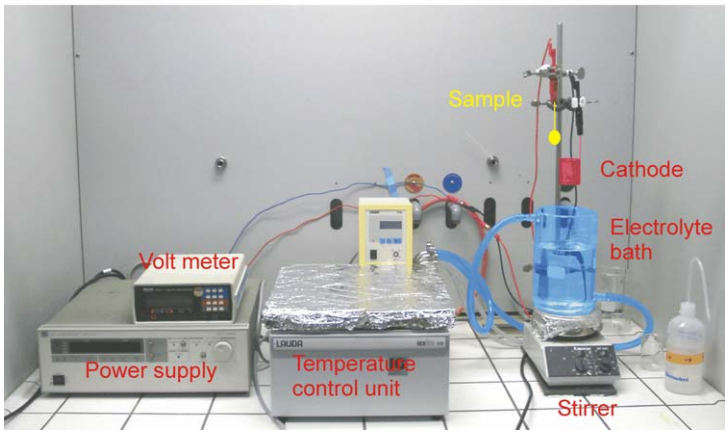

Figure 1.5 APC Treatment of Screws. Equipment used for the anodic plasma chemical process (Frauchiger, PhD thesis).

The coating setup for the APC process is similar to that used for conventional anodic oxidation. The main difference is that the voltages can go up to 500V, while supplying high currents at the same time. The titanium formed a natural oxide layer initially followed by an anodic oxide film, once a high positive voltage had been applied. The characteristic "sparking" in the anodic spark deposition method was then produced due to a dielectric breakdown of the oxide layers. At this stage there was localised melting (fusion) of the oxide and the titanium substrate, incorporating ions from the electrolyte solution in the formatted layer. This localised melting weakened the surrounding area, causing a cascade of reactions and resulting in the production of a porous layer containing both titanium from the anode and the electrolyte ions. This method converted the pure metal oxide layer into an armorphous coating of mixed oxide and Ca-P in a continuous process. (details of this method were obtained from Schreckenbach *et al*., 1999 and Vinzenz Frauchiger, PhD thesis, 2002).

In this process, it is possible to create a thicker titanium oxide layer with a controlled porosity. The four APC test surfaces were a mixed layer of titania and Ca-P, produced at 249 and 360mA in a newly developed Ca-P electrolyte system (Frauchiger, PhD thesis, 2002) and a titania layer (containing phosphate) produced in a phosphoric acid electrolyte at 25°C and 75°C. Figure 1.6 shows a diagrammatic representation of the events in the procedure described above.

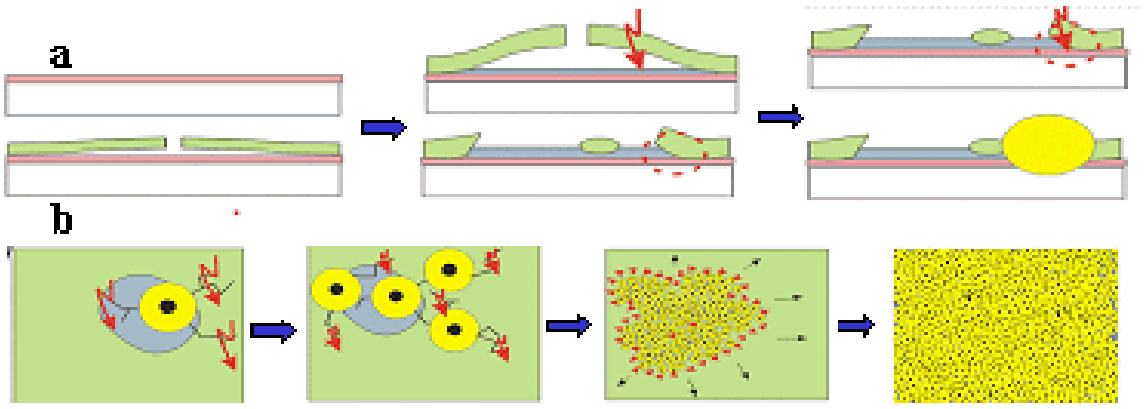

Figure 1.6 Diagrammatic representation of the events of film formation in anodic plasma-chemical treatment of a surface from the side (a) and above (b) (Frauchiger, PhD thesis, 2002), resulting in the formation of the surfaces seen on the screws. Phase 1 – formation of an anodic oxide layer, blister formation and first breakdown events, followed by higher energy breakdown events giving a thicker oxide with the APC structure and finally the breakdown events spread over the surface until the whole sample is coated.

2. Materials and Methods

2.1 Screw Surfaces.

A set of coated and uncoated SYNTHES® 4.5mm titanium grade 4 cortex screws (Figure 2.1), ref: 414.016 were evaluated in this biocompatibility study. Anodic plasma chemical (APC) treated with electrolytes of Ca-P at current densities of 200mA & 290mA; APC treated with electrolytes of 0.01M phosphoric acid (APC-P) at temperatures of 25ºC & 75ºC; anodised to produce an oxide of gold colour (control, as used in SYNTHES® osteosynthesis implants); coated with HA by plasma spraying, as a negative control (VPS); coated with HA by cool method spraying, as a negative control (bmim). Unfortunately the production details for the two HA control surfaces were not divulged by the supplier. The APC-P and VPS coatings are non soluble layers. All screws were sterilised (35.2 kGy) before use.

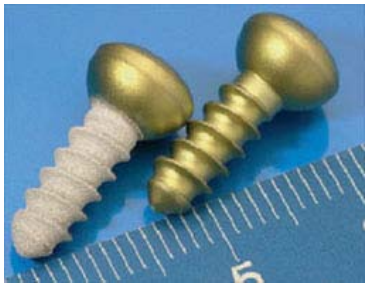

Figure 2.1 Left side: coated and right side: standard non-coated cortex screw

2.2 Surface Characterisation

Scanning Electron Microscopy

Screw surface topographies were imaged using high current backscattered electron (HC-BSE) imaging (Richards and Gwynn, 1995) with a Hitachi S-4700 Field Emission Scanning Electron Microscope (FESEM). The images were taken using an accelerating voltage of 5kV, an emission current of 50μA, a condenser lens setting of 16 and an objective aperture of 1. An yttrium aluminium garnet (YAG) detector was used to produce BSE images.

Laser Profilometry

Non-contact laser profilometry was used to quantitatively determine the samples height profiles. The surfaces were measured with a UBM laser profilometer (UBM Messtechnik, Germany) with a microfocus™ sensor. The vertical resolution was 10 nm with a measurement range of ±50 mm. Ra and Rmax were measured from a 0.5mm x 0.5mm analysis area scan between screw threads at 500 points per mm. Prior to roughness calculations a linear regression to eliminate surface inclinations was performed on each profile.

X-ray photoelectron Spectroscopy (XPS)

The chemical composition of the screws at the surface was measured using X-ray photoelectron Spectroscopy (XPS) on a SAGE 100 (Specs, Berlin, Germany). The XPS used non-monochromatic MgKα radiation with an energy of 240W (12kV, 20mA), an electron take-off angle of 90°, and an electron detector pass energy of 14eV for detail spectra. The screws were always measured in the middle of the thread. All peaks were referenced to the C_{1s} (hydrocarbon C-C, C-H) contribution at 285eV.

2.3 *In vivo* methods

Groups: Eight adult female white Swiss alpine sheep, from a single breeder, of age between 5 and 6 years, weight between 66 and 76 kg, all in good health, were chosen for this study and examined over a twelve-week observation period. All experiments were approved by the Animal Experimentation Commission of the Canton of Graubuenden, Switzerland (Swiss Federal Legislation, Animal Permit GR 3/2001).

Figure 2.2 White alp sheep in the laboratory animal stabling

Animal pre-surgery preparation: Sheep were fasted 24h before surgery with free access to water. The animals were sedated with Valium® (Diazepam) at a concentration of 15 mg/sheep. A venous catheter (Vasofix® 18 G, Braun Medical) was placed in the left jugular vein to infuse Ringer lactate at a concentration of 12ml/kg/h during the whole procedure. Induction was accomplished with 5% Thiopental at a concentration of 350mg/sheep. Pre-emptive analgesia was achieved by a single slot spinal anesthesia with Xylazine (Rompun®) at a concentration of 0.05mg/kg. After intubation, anaesthesia was maintained by isoflurane in a N_2O: O_2 mixture with a 2: 1 ratio using a semi closed system. A naso-gastric tube was inserted in the sheep to prevent a gas accumulation of the rumen and subsequent regurgitation. The animals were prepared in a separate room before they were brought to the surgery room. Equipment used: Betadine®, Jodobac®, swab, Peha-haft® (elastic bandage), shearing clipper. The sheep were placed on their right side. In the region between the pastern and the distal part of the femur the fleece was shaved. This region was cleaned three times with 50% Betadine®-

solution and then dried with swabs. The lower part below the pastern was covered with a bandage. Then the sheep were turned into dorsal recumbency and the surgery areas of the legs were sprayed with Jodobac® detergent.

Surgical Procedures: The operative procedure was performed under assisted general anaesthesia. Postoperative analgesia was achieved with Carprofen (Rimadyl®) at a concentration of 4 mg/kg after surgery and also on the following day.

Figure 2.3 Sheep connected to the isoflurane inhalation anaesthesia system.

A 7-hole-PCfix implant was placed on the skin as a stencil to judge how long the incision had to be. Subsequently, a 12 cm incision was performed at the medial aspect of the tibia in the midshaft region with a surgical blade #10. The following preparation was performed with a #15 surgical blade and with a scissors until the periosteum was reached. An important consideration was good haemostasis and to leave as many vessels untouched as possible. Screw location was varied within a template in each sheep (Fig 2.4) so that each screw type had been placed once in each location within the template. The position for the screw holes was marked using a blade on the periost through the holes in a PC Fix implant as a template (Fig 2.4). The screws holes were drilled with a small AO air drill, with a drill guide, cooled with sterile ringer solution. In total, seven 3.2mm diameter holes were drilled with the drill bit protected by the corresponding drill guide, vertical to the tibia surface. The first hole was drilled and the first screw inserted after measuring the cortex thickness and cutting the threads with the tap (4.5 mm) (Fig. 2.5). The thread hole was tapped to cut the threads into the cortex. Every hole was rinsed with sterile 0,9% NaCl solution (Fig. 2.6). The screws were inserted with the screwdriver until the screw head touched the bone (Fig. 2.7). The screws were then released two turns from the cortex. With the torque sensor key (Fig. 2.8) the screws were then driven four half turns in and the torque data was recorded with the Adwin gold A/D converter. The insertion torque was measured. The instrumented screwdriver was used to turn the screws four half turns into the bone.

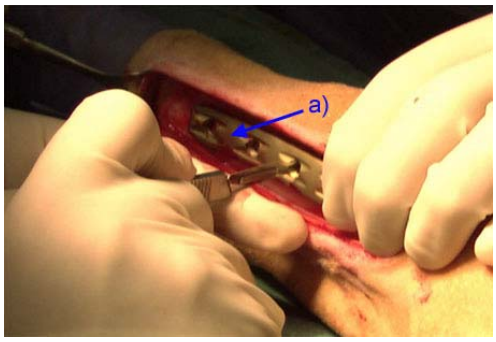

Figure 2.4 Marking position for the screw holes.
a) PCfix implant

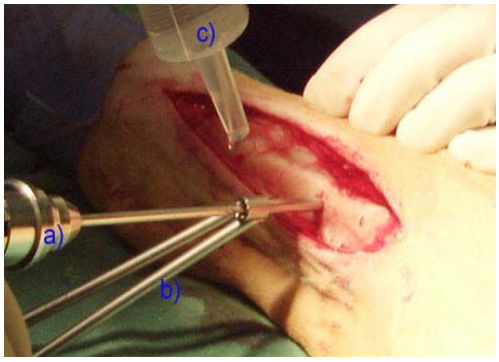

Fig 2.5 Drilling (and setting the screws).
a) Small AO Air Drill,
b) drill guide
c) ringer solution

Figure 2.6 Tapping of the thread hole.

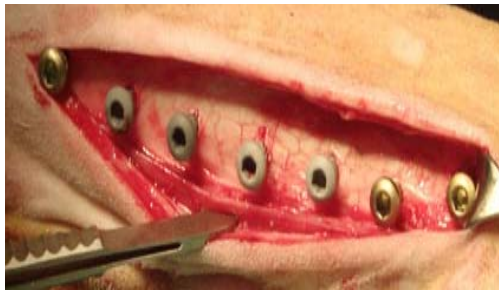

Figure 2.7 Setting the screws.
All seven screws are seen in their implantation sites (right side = proximal).

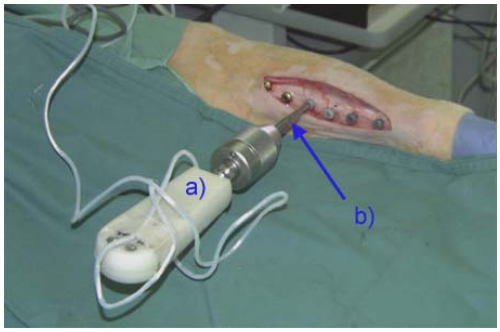

Figure 2.8 Torque measurement.
a) Torque sensor key
b) special produced screwdriver

Closure of the wound: The wound was rinsed with sterile 0.9% NaCl the fascia closed with a Vicryl® 2-0 (polygalactin 910, braided, resorbable, continual suture), and the skin closed by an Ethicrin® 4/0 (polyamide, monofilament non-resorbable, vertical mattress suture). Thereafter the skin was cleaned with sterile NaCl 0.9% and final disinfection was performed with Jodobac®. A pressure bandage was applied for 10 min with swabs and cloth clamps. For 2-3 days protective bandages with gauzes and Jodobac® were applied directly on the suture and held in place with an elastic bandage (Peha-haft®). The same procedure was repeated on the other hind leg.

Follow-up: Postoperative analgesia was achieved by administration of 4mg/kg Caprofen (Rimadyl®) the following day. Immediately post-surgery and for the first week of the observation period, all animals were housed in individual boxes in protection slings (hammocks) that allowed full weight bearing on the legs but not reclining. The goal of this was to minimise the possible damage to the implant sites. For another two weeks each sheep was kept in a single box (Figure 2.9) to minimise the complication risk and to facilitate wound-control.

Figure 2.9 A sheep immediately after surgery well-positioned in support.

Fluorescent bone growth marker: To evaluate the new bone growth over time, two different fluorescence markers were injected subcutaneously into the sheep during the bone healing process. One injection was in the fourth week post operation: Xylenol orange (Rahn & Perren 1971) at a concentration of 90 mg/kg. A second injection was at eight weeks post operation: Calcein green (Suzuki & Mathews 1966) at a concentration of 5 mg/kg.

Radiography: During the whole *in vivo* experiment radiography images were taken of both hind legs at two week intervals.

Implant-Bone removal: After twelve weeks, the animals were sacrificed with an overdose of Pentobarbital (Vetanarcol®). Extraction of the lower limb was at the knee level (Bone with muscles). After this the bone was freed from the muscles with a scalpel.

2.4 Mechanics

Torque measurement

Torque measurements of screw extraction were taken to study bone anchorage of screws. Material: Adwin-Gold: (Jäger-Computergesteuerte Messtechnik GmbH, Lorsch D) Matlab: (Mathworks GmbH, Schürmattstrasse 6+8, 3073 Gümligen). Instrumented screwdriver (Type Rumul, Russenberger AG (no longer exists), modified by D. Wahl, AO Research Institute)

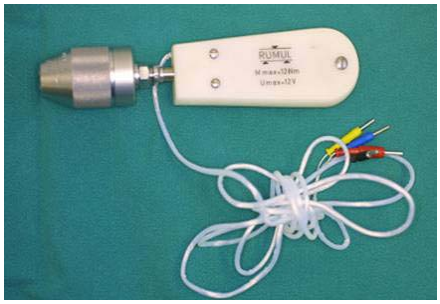

Figure 2.10 Sensor screwdriver. It is possible to use different drives for different screws (Cortical screws, Schanz screws).

Digital torque key: Calibration of the sensor was performed with the help of a digital torque key. This calibration was necessary for the conversion from volts into Nm. Shortly after the sacrifice of the sheep screw extraction torque measurements were conducted. After removal the tibia was fixed in a bench vice where the screws were removed from the tibia with the help of the torque screw driver. After converting of the measurement data with the Matlab-program, curves were obtained with four peaks at insertion torque and a curve with four peaks at extraction torque (Figure 2.11).

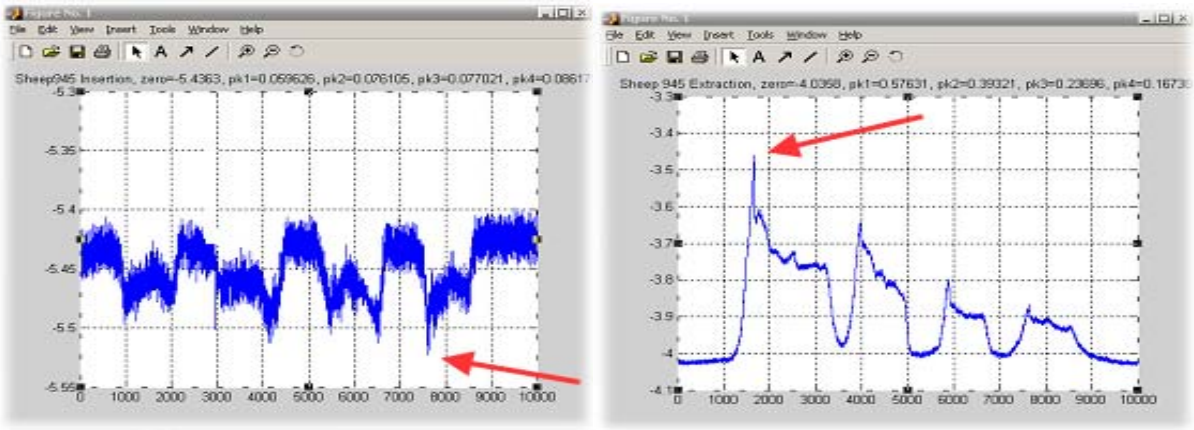

Figure 2.11 Left is an example of a curve for the insertion torque measurement. The red arrow shows the "final insertion torque". On the right is an example of a curve for the extraction torque measurement. The red arrow shows the "initial extraction torque".

The final insertion torque-peak represented the insertion torque for final anchorage at the time of surgery. The first three insertion torque peaks represented the friction during the manual insertion process. The initial extraction torque-peak represented the extraction torque for

initial anchorage at week 12 post operatively. The following three extraction torque peaks represented the friction during the unscrewing process.

2.5 Radiography

Radiographic analysis: Standardised radiographs, in the plane of the screws, were taken immediately after surgery. The ensuing radiographs were made at intervals of 2 weeks until euthanasia at 12 weeks post operation and cortex thickness on each screw surface monitored over time. Radiographs were taken of each leg. To compensate the different bone shapes of the proximal part two radiographs were taken at different projections. The aim was to compare the cortical thickness at different times of the healing process. The screws had to be radiographed at a correct angle on the radiography film (Kodak Diagnostic film, InSightTM, IS-1, 18 x 24 cm), to see their full length. Technique: 55kV, 16mAs exposure time cranio-caudal direction. The sheep was lying on the right side and was not changed during the radiography process for both hind legs. Only the height of the table was changed.

Radiography image analysis

Material: Digitising: Scanner (Epson; model EU-35), Adobe Photoshop 6.0, PC-image analysis and measurements program (Foster Findlay, Newcastle GB).

A mask in the Adobe Photoshop program was used to cut out the area of interest (Figure 2.12). The endosteal callus formation next to the screw tips was measured in length during the 12 weeks of the healing process. The callus area next to the screw head was not considered (some screw heads were fully coated, some partially and some not coated at all). Due to the inadequate quality of the standard X-ray films the density of original bone next to the screw shaft (remodelling zone) was not suited for measurement. The diameter of the original cortex was measured at week 2 with regard to any correlations to the callus formation or the torque measurement.

Figure 2.12 An X-ray image with fitted mask. All screws and the X-ray wedge were included.

Contact-radiography

Material: Faxitron 804 (Faxitron Company, IL 60089; USA), Film: AGFA Structurix D4, film size: 24x30 cm, aluminium step wedge 0.5mm-9mm, film-focus distance level 4 (30 cm), filter: 0.5, Radiography : 30kV, 2min 30s exposure time.

Contact radiography was used to identify good specimens for further processing. An overview exposure of the histological slides (thickness of 200 24µm +/-30 µm) was made.

Figure 2.13 Open Faxitron with a prepared X-ray film inside.

Image Analysis (ZEISS KS 400)

Material: (ZEISS) Digitising: AxioVision 3.0 program, Axiocam, Objective (diaphragm open): Luminar 40 plus C-mount adapter plus 30mm intermediate ring, scale bar (accurate to a tenth); KS 400 program. The region of interest to quantified was the callus formation next to the screw tip. The screw images were digitised with the Axiocam camera combined with an objective. The display window was sized so that the whole callus formation next to the screw tip was included. The ZEISS KS 400 measurement program was used for interactive evaluation with a self-written macro (see Appendix). A mask was created which included only the callus formation, the whole screw tip and medullary canal (Figure 2.14)

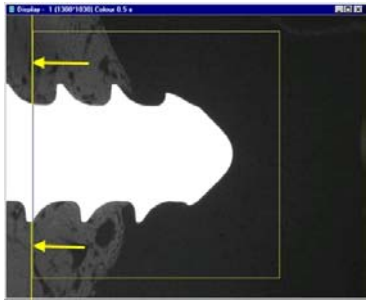

Figure 2.14 The mask is placed at the border between the original cortex and the callus formation (yellow arrows)

It was not possible to include the whole callus formation (Figure 2.14) proximal and distal of the implant since a part of this was lost during the rough histological preparation. Three areas inside the mask could be measured by a threshold technique: Screw area, callus formation area and medullary canal area.

2.6 Histology

Bone apposition onto the surfaces at 12 weeks was measured, after histological preparation, with bright field light and fluorescence microscopy.

Pre-fixation sample preparation

The right hind leg of every sheep was used for histology. The tibia was cut into sections (2 cm) with a band saw (BIZERBA, Latscha, CH-Zürich), one for each screw.

Figure 2.15 Cutting procedure with the band saw

Fixation / Embedding

Reasons for Fixation: The purpose of fixation was to preserve all components of the bone tissue sample in as near to natural situation as possible, without diffusion of constituents. The tissue had also to be protected from osmotic damage. The processes of autolysis and bacterial attack had to be prevented. A poor fixation is irreversible and affects structure, shape and volume during the subsequent procedures. Fixatives should not interfere with subsequent staining of sections.

Procedure: Formalin, a crosslinking fixative (aqueous solution of formaldehyde) buffered with sodium phosphate at pH 7.4 was used at 4% for +/-12days at 4°C. Buffered formalin is used for all kinds of soft tissues and staining as well as for undecalcified bone including specimens, which underwent fluorochrome labelling. The advantage of using this fixation is that the buffer keeps the pH from turning acid, which would damage the calcium-bound fluorochrome staining

Embedding in methyl methacrylate (MMA): To obtain uniform, thin sections, the material must be of certain hardness and of uniform stability. This is achieved by impregnating bones and tissues with a liquid medium, which hardens to a homogeneous mass. This procedure is called embedding. The embedding medium is deposited wherever there is space, in particular where water has been removed.

After fixation in the formalin and washing in water (1 day), the specimens were transferred stepwise to the final solutions (twice changed in 3 days, 4°C): 40%, 80%, 96%, absolute

ethanol, followed by Xylenol for 3 days. Specimens were then placed through embedding media as follows: MMA I (pure MMA) for 3 days, (room temperature), MMA II for 3 days (4°C), MMA III for 1-4 weeks (first at 4°C, afterwards 20° water bath). (MMA I: MMA pure, MMA II: MMA plus Benzoyl peroxide (catalyst), MMA III: MMA plus Benzoyl peroxide (catalyst) plus Dibutyl phtalate (softener))

Sectioning

Screw location was identified in the embedded specimen, with a radiography image-amplifier (Arco Spot Imaging, Via E.Fermi 25/A-24066 (BG) Italy) at 53kV, 10mAs (exposure time) for the first cut for the diamond-saw blade (0.2 D91, thickness: 500µm) on the CP 310 EXAKT-saw (EXAKT Apparatebau, D). The screw shaft thickness was 4.5 mm, which resulted in four 200 µm thick cuts from every screw and the surrounding bone.

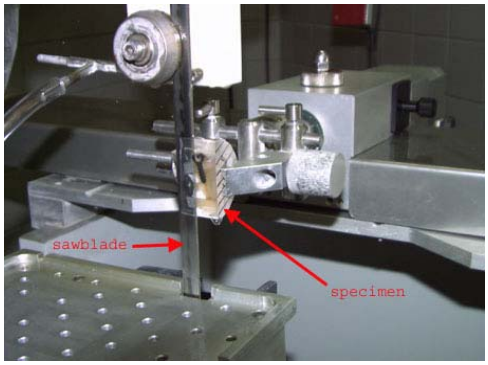

Figure 2.16 EXAKT-saw with MMA embedded specimen, titanium screw implanted in bone material (arrow) cut by a 0.2 D91-diamond saw blade with cooling through normal water.

Preparation for light microscopy

The samples were glued on plastic object slides with Cyanolit® and then ground to a 100 µm thickness using the EXAKT-Grinding machine (EXAKT, Haska, CH-3000 Bern)

Silicon Carbide (SiC) paper 1200. Afterwards they were polished for 10 min with SiC-paper 2400 followed by 10 min with SiC-paper 4000.

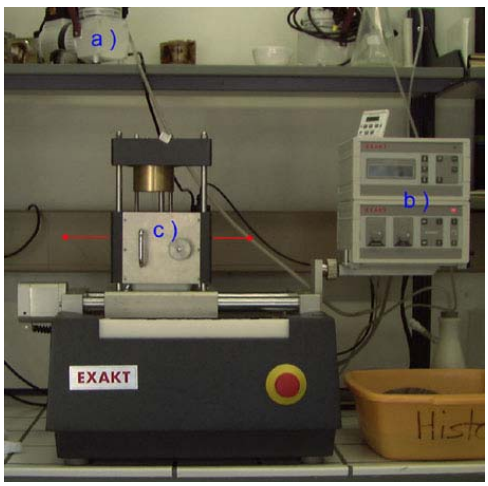

Figure 2.17 EXAKT-Grinding machine: Vacuum pump a); a vacuum was produced to keep the plastic object slide in touch with the sliding table c). Control unit b) for rotation speed of the grinding plate and speed of the movement (red arrows) of the sliding table.

Staining

Sections were placed in 1% formic acid for 20-30 seconds, followed by rinsing in running water for 5-10 min. Slides were blotted with filter paper, placed in preheated 15% Giemsa (57C°) stain solution for 20 min, and briefly rinsed for a few seconds in demineralised water. The specimens were checked by eye whether the stain had taken adequately and then rinsed twice in 96% ethanol, ten times in 100% ethanol and the slide was blotted with filter paper.

2.7 Light Microscopy

Qualitative light microscopy

The qualitative light microscopy aspects were used to get an idea of what happens in the different areas along the screw/bone interface with the fluorescent- and the Giemsa samples. Specifically the area was determined in which the quantitative evaluation was to be performed. The screw/bone contact zone was divided in four parts (Fig. 2.18).

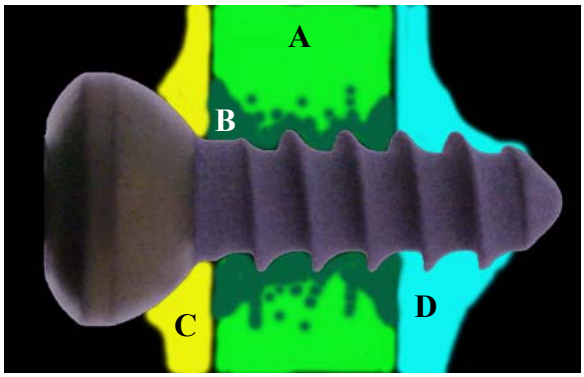

Figure 2.18 Areas of interest
A: cis cortex without remodelling (area of old bone). B: remodelling area within cis cortex (area with dead bone without blood supply and new bone formation). C: new bone growth around the head. D: new bone growth around the screw tip

Quantitative light microscopy evaluation

Bright field microscopy

Material: (ZEISS) Digitising: Axioplan 2, Axiocam, AxioVision 3.0 program, Objective Plan-Neofluor 5x Art. 4403 20; Measurement: Axiovision 3.0, program (ZEISS).

Using Giemsa staining the proportion of mineralised screw contact was analysed. This was performed for the remodelling as well as for the callus area. The fraction was calculated as a ratio between calcified length and total length (calcified length and gaps). Using the Objective Plan-Neofluor 5x of the Axioplan 2 microscope the samples were imaged in overlapping areas. The length measurement tool of the Axiovision programme was used to measure the bone contact zone (calcified bone) along the implant surface. The remodelling area (original bone) and callus formation area were distinguished using the same measurement technique. All the gap zones and calcified contact zones were measured along the screws.

Definition: a) calcified contact zone - no osteoblasts or soft tissues between calcified bone and screw surface. b) gap-zone – osteoblasts and or soft tissues between calcified bone and screw surface.

Fluorescence microscopy

Material: (ZEISS) Digitising: Axioplan 2, Axiocam, AxioVision 3.0 program, Objective Plan-Neofluor 5x. Measurement: KS 400 program (ZEISS), Adobe Photoshop 6.0

The amount of bone formation was calculated as marked area divided by total area of the image minus screw area. With this evaluation it was possible to gain information on the increase of callus formation next to the screw at week 4 and 8 post-operatively. The region of interest for quantification was the callus formation next to the screw tip. For both fluorescent markers, the same technique was used. Blue excitation was used to show green fluorochromes from Calcein green (Zeiss filter set # 10: exciter filter: BP450-490, beam splitter FT 510, barrier filter BP515-565). Green excitation was used to show red fluorochromes from Xylenol orange (Zeiss filter set # 15: exciter filter BP546, beam splitter FT 580, barrier LP 590. Position 3). Three band excitation was used to show red, green and blue fluorochromes. (Zeiss filter set # 25: exciter filter TBP 400/495/570, beam splitter FT 410/505/584, barrier filter TBP 460/530/610).

With the Objective Plan-Neofluor 5x of the Axioplan 2 microscope the samples were imaged. Afterwards the images were processed in Adobe Photoshop 6.0. The first image was taken at the border of the callus formation. The height of the image was defined by the highest thread. The image included only areas with fluorescent bone. The KS 400 measurement programme was used for interactive evaluation by a self-written macro (see Appendix). The threshold was set to include all fluorescent structures labelled by the two fluorochromes.

2.8 Data analysis (statistics)

Material: All statistical analyses were carried out using SAS, Version 8.0

Analyses and regression models:

Differences between screw types were examined with general linear regression models. The SAS Procedure PROC MIXED was used considering correlation within observations using autoregressive AR(1) models to account for covariance across positions or time-points, respectively. Alternatively, animal effects were considered as random effects to account for

inter-individual variation (i.e. between animals). Multiple comparison tests were adjusted by the methods of Tukey and Kramer.

The distribution of the residuals was evaluated using qq-plots and Tukey-Anscombe plots (residuals against predicted). Furthermore, tests for normality were carried out using the Shapiro-Wilk test. Least Squares Means are computed to describe model-adjusted effects (Searle, S.R. Speed, F.M. and Milliken, G.A. (1980)).

Growth rate of cortical bone thickness between week 0 and week 12

A logistic growth curve had to be fitted individually for each combination of the following, specific animal, side (left or right), position of screw, and screw type i.e. 7 time-points were used for each single regression. Therefore, all together, 105 models had to be fitted (7x2x7=98 + 1*7 = 105), Sheep number 980 had left side values only (because of infection on right leg). One explored These fitted parameters were explored to make any statement about statistical differences. Structure of the model:

$$cortex = \frac{a}{1 + \exp(b + c * week)}$$

If factor ‘week’ goes towards infinity, the denominator becomes 1, thus the plateau value parameter ‘a’ will be reached. The parameter ‘c’ expresses the rate of change, where as ‘b’ is a nuisance parameter, i.e. the intercept for week=0.

3. Results

3.1 Surface Characterisation.

Scanning Electron Microscopy

There were four types of APC screws tested (Figs. 3.1 – 3.7). Two types of these APC screws were modified by V. Frauchiger (see fig. 1.5 and 1.6).

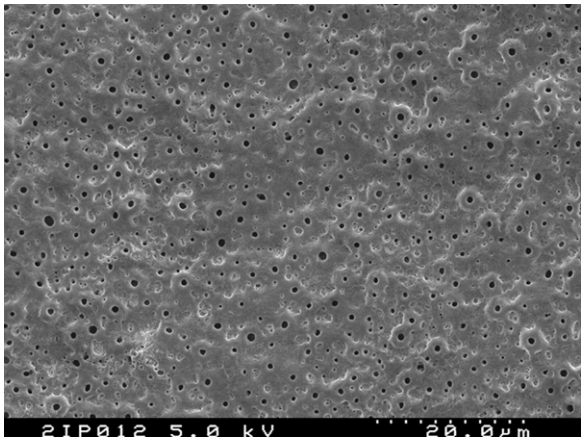

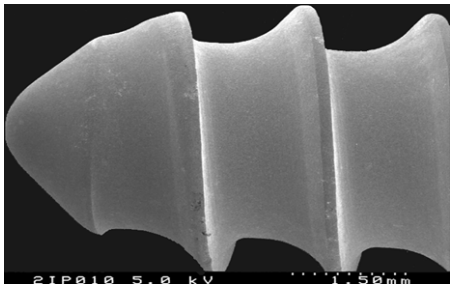

Figure 3.1: APC-CaP-249 CpTi screws (APC coating: 6 µm +/-1, 249 mA, 90s at 25°C, porosity higher than at 360mA)

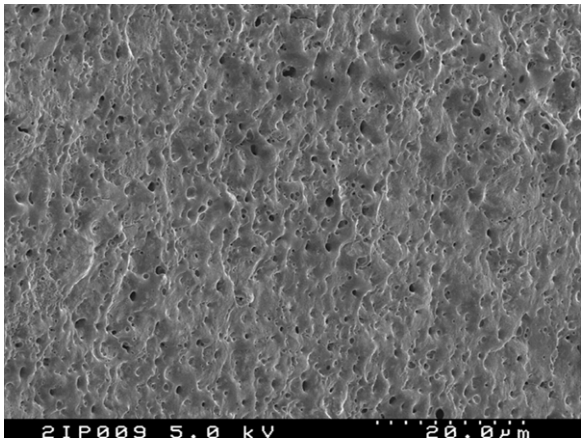

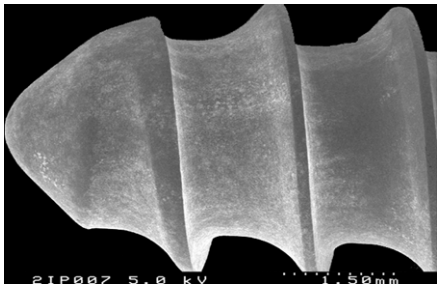

Figure 3.2: APC-CaP-360 CpTi screws (APC coating: 6 µm +/-1, 360 mA, 90s at 25°C)

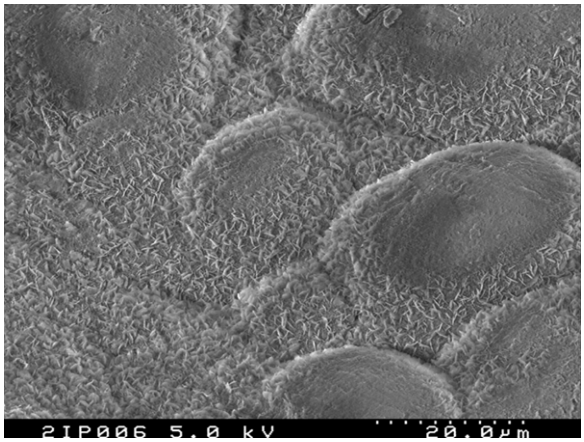

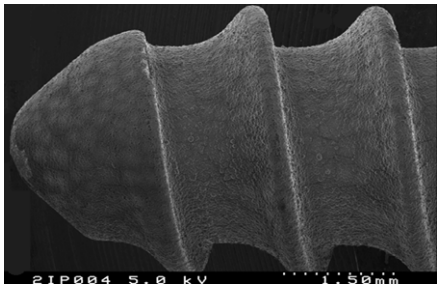

Figure 3.3: Bmim CpTi screws (biomimetic-coating: 40µm, CaP-crystallized surface)

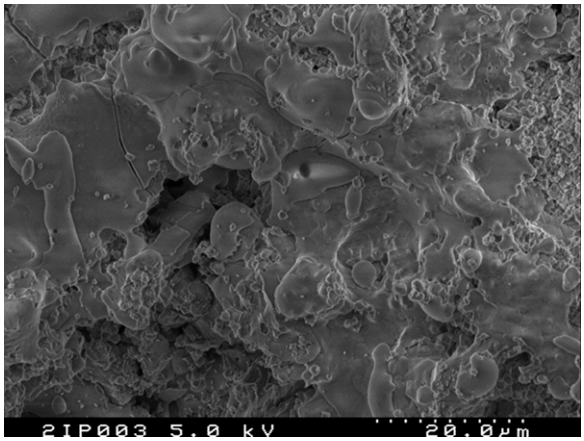

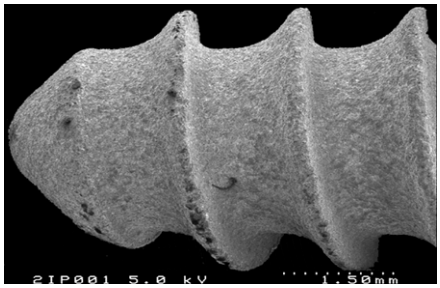

Figure 3.4: VPS CpTi screws (HA–plasma-coating: 30 µm)

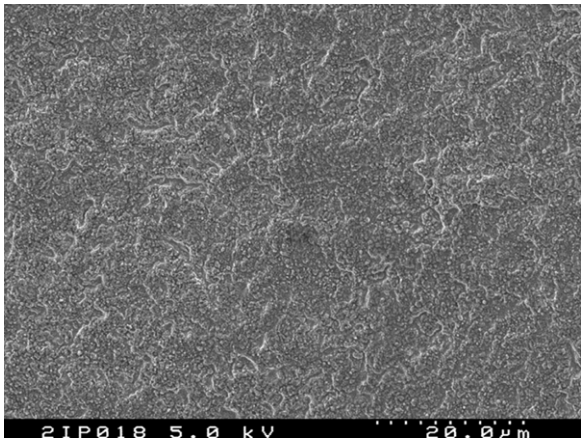

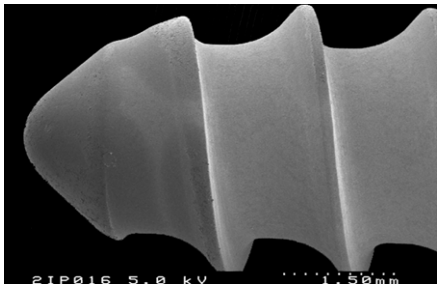

Figure 3.5: APC-P-25 CpTi screws (APC-coating: 2-3 µm , made in phosphoric acid bath at 25°C)

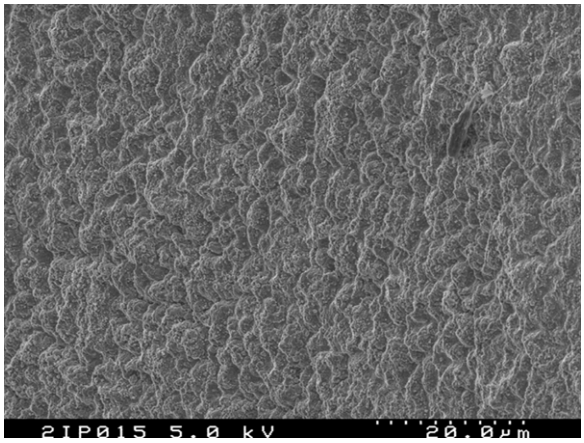

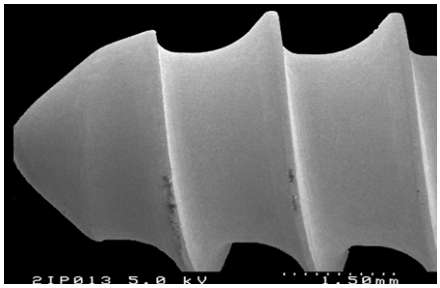

Figure 3.6: APC-P-75 CpTi screws (APC coating: 2-3 µm, made in phosphoric acid bath at 75°C)

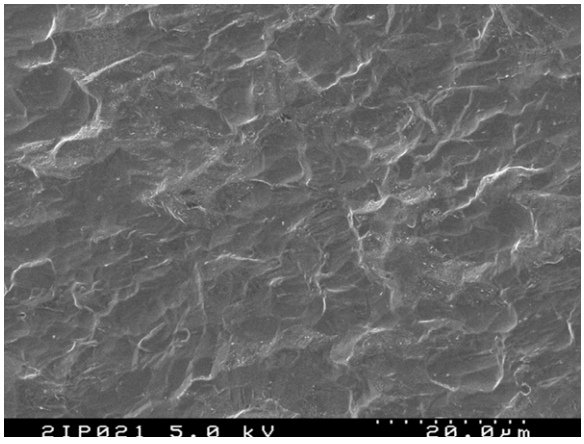

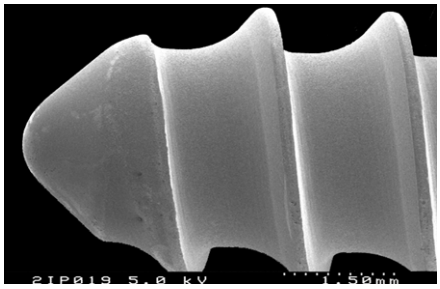

Figure 3.7: CpTi screws (standard anodised titanium, without coating)

The Standard Error to the Mean (SEM) was used to qualitatively investigate the surface morphology of the coatings. The morphological differences between all the coatings and non-coated control are clear. The porosity of the APC Ca-P coating at 249 mA was much greater than at 360 mA and the pores were also more regularly distributed over the surface. The APC–P surface (produced in 0.01M phosphoric acid) at 25°C had a smoother looking surface than the one produced at 75°C, which appeared coarse and 'bumpy' looking. Bmim had a crystalline structure and VPS had a very rough and coarse non- crystalline structure. The standard anodised titanium, without coating was not porous and appeared to have less microroughness than the coated surfaces.

Profilometry

The roughness values of the screw surfacees, as determined by laser profilometry in general, follow what was observed with the morphological images from the SEM, with bmim and VPS having the highest roughnesses (Table 3.1). What the profilometer does not show, since it gives lower roughnesses for the APC surfaces compared to the uncoated titanium surface, are the pores observed in the SEM images, since the laser profilometer does not resolve features below about 1.5μm.

Screw Type	Ra (μm)	Rmax (μm)
Uncoated, but anodised CpTi (UNT)	1.05	12.43
HA-coated, chemically deposited (bmim)	6.83	78.3
HA-coated, plasma sprayed (VPS)	3.41	32.17
Phosphoric acid (H_3PO_4) APC coated at 360mA at 25ºC	0.58	6.35
Phosphoric acid (H_3PO_4) APC coated at 360mA at 75ºC	0.58	6.72
CaP, deposited using APC treatment at current density of 249mA	0.55	8.62
CaP, deposited using APC treatment at current density of 360mA	0.53	5.91

Table 1. Table showing the Ra and Rmax values recorded by laser profilometry for the various surfaces. Ra- centre line average represents height or arithmetic average of the absolute values of all points of the profile. Rmax - Maximum individual roughness depth. Bmim and VPS coated screws are observed to have a much greater Ra and Rmax than all other surfaces. The APC treated surfaces were all in a similar range of roughnesses.

XPS

The chemical composition of the outermost few nanometres was determined semi-quantitaively using XPS. The chemical compositions of the different coatings can be seen in Table 3.2. As expected in the APC coatings C, Ca, O_2, P and Ti were found at or near the surface. Ti was not observed at the coating surface of either HA control. The presence of C is due to contamination from ambient air.

	Carbon	Calcium	Oxygen	Phosphorus	Titanium	Sodium	Minor
HA_VPS	34.2	15.8	37.5	12.5	0.0		Na
HA_bmim	9.1	20.9	53.7	16.4	0.0		Na
APC H_3PO_4_25	32.3		47.0	12.2	8.4		Na, N
APC H_3PO_4_75	34.8		44.9	12.7	7.6		Na, N
APC CaP_249	19.4	8.8	51.5	8.8	8.8	2.7	
APC CaP_360	23.1	9.9	48.6	8.7	7.1	2.5	

Table 3.2. Chemical composition of the screw coatings at the surface (XPS measurements). Comment: The HA coatings and the APC H_3PO_4 coating contain carbon as major contaminant while for the APC (Ca-P) screws (new electrolyte) carbon is also contained in large amounts in the electrolyte. The level of carbon as a contaminant can vary to a very large extent. As soon as the screws are exposed to air they get contaminated. Differences in the carbon level from surface to surface are difficult to explain. Nitrogen is also a contaminant from the process. The same is true for sodium. But Sodium is present in the APC electrolyte and is therefore expected to be in the APC coatings

3.2 Mechanics

Torque measurements

The torque at insertion showed equal values (not significantly different) and the torque level at insertion was always significantly smaller than the torque level at extraction for all tested screw types. In addition there was no correlation between torque level at extraction and torque level at insertion. The mean of the torque at insertion ranged between 0.07-0.11 Nm (not significant) (Fig. 3.8). The mean of the torque at extraction ranged between 0.58-0.83 Nm (14 out of 21 values were significant).

Torque at insertion (statistics): The data showed increasing variance with higher values, which made a logarithmic transformation necessary. A model of the form $Y=\alpha + a(animal) + \beta pos + \delta_1 screw + e$ (a=animal, pos=screw position in the tibia, screw=screw type, e=statistical variable), where a(animal) was treated as random effect, was examined. There was only a small effect due to screw type but there were no significant differences at insertion torque

among the different screw types. Finally was concluded that torque at insertion was similar for every screw. ($p > 0.05$). Therefore the focus was placed just on the extraction torque.

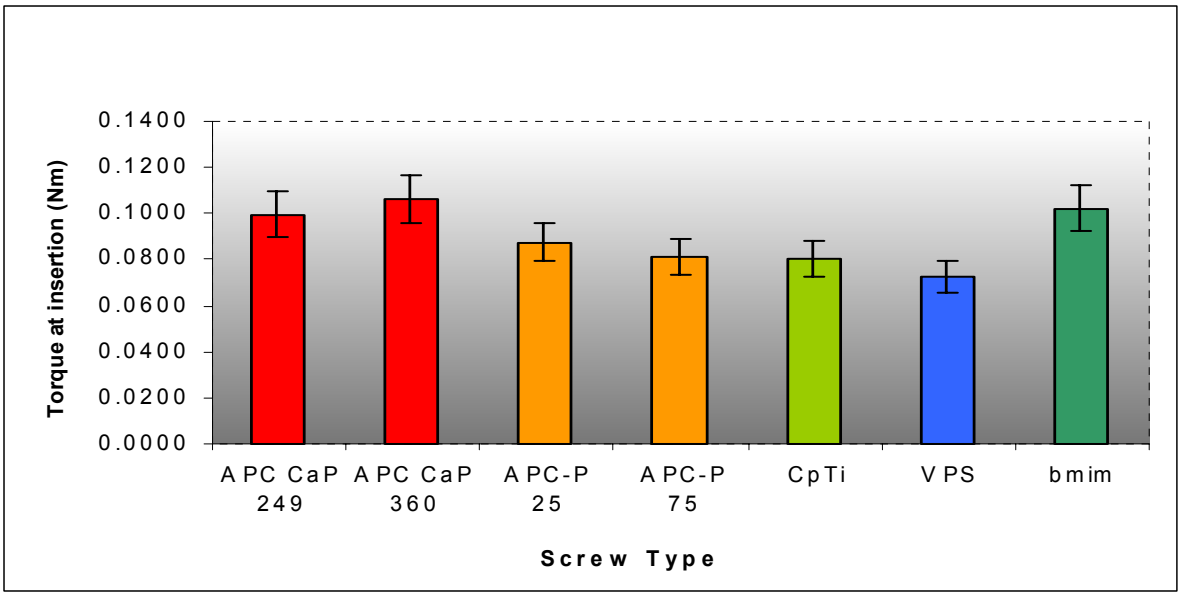

Figure 3.8 Insertion torque at implantation for all seven screw-types. After Tukey and Kramer statistical tests the screws show equal torque values at insertion. The values are least square means adjusted for the animal variations and position of the screw in the tibia by statistical analysis, +/- standard error are shown.

The screw types coated with HA exhibited significantly higher extraction torques than all other surfaces (Fig. 3.9). VPS showed (statistically significant) the highest torque level at extraction (Fig. 3.9). Bmim showed (statistically significant) the second highest torque level at extraction (Fig. 3.9). Third highest torque was shared by APC-CaP-360, APC-CaP-249, APC-P-25 (all the same torque levels at extraction), which was significantly higher than CpTi (Fig. 3.9). The torque at extraction of APC-P-75 was also higher than CpTi (but not statistically significant) (Fig. 3.9). CpTi showed the lowest torque at extraction level (Fig. 3.9).

Torque at extraction (statistics): Among the torque at extraction measurements were three extreme observations that needed to be excluded from the data to hold the model assumptions of normal distribution. After excluding these observations, the residual pattern was compatible with normality. A model of the form $Y=\alpha + a(\text{animal}) + \beta\text{pos} + \delta_l\text{screw} + e$, where a(animal) was treated as random effect, was examined.
There was a negative but not significant correlation ($r= - 0.24$) between torque at extraction and Cortex thickness. (Correlation with model based extraction: There was no correlation between extraction and cortex thickness). Due to the fact that the animals were taken as random effect, the presented results of the extraction torque should show the differences between the screws.

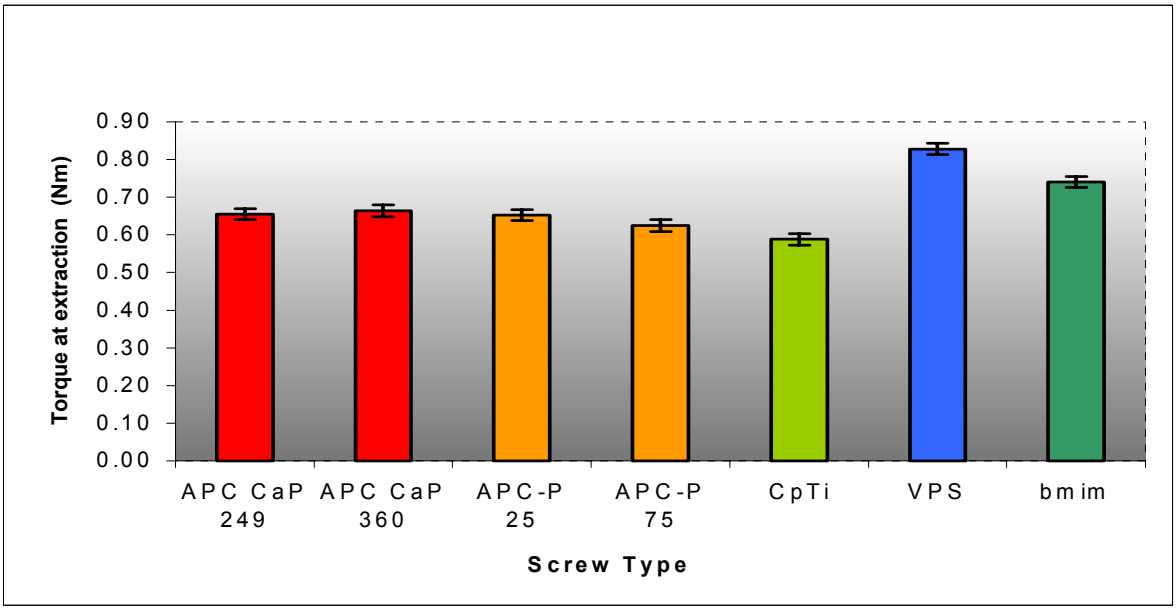

Figure 3.9 Extraction torque 12 weeks after implantation for all seven screw-types. 14 out of 21 comparisons show significant effects: The values are least square means adjusted for the animal variations and position of the screw in the tibia by statistical analysis, +/- standard error are shown. VPS to all other screw types. Bmim to all other screw types. APC-CaP-360 to VPS, bmim, CpTi. APC-CaP-249 to VPS, bmim, CpTi. APC-P-25 to VPS, bmim, CpTi. APC-P-75 to VPS, bmim. CpTi to VPS, bmim, APC-CaP -360, APC-CaP -249, APC-P-25.

3.3 Radiography

Radiography *In vivo*

The *in vivo* radiography images facilitated differentiation between original cortical bone and callus / *de novo* bone formed around the screw head and the screw tip on the endosteal side (figure 3.10 and 3.11). These measurements were used to plot a growth rate chart of cortical bone thickness between week 2 and week 12 of the various screw surface types (figure 3.12). It was established that that the statistical growth rate model could not be fitted adequately to the growth rate data, and other ways to assess the growth rate needed to be found. To this end, the differences between growth at week 4 and 6 were used as an indicator of growth rate (figure 3.13). There was no indication observed for a different bone growth rate between the tested surfaces. Radiographic measurements at week 12 gave an idea about the bone growth situation at the end of the *in vivo* testing (figure 3.14). Five out of 21 comparisons between the samples showed significant effects: APC-CaP-249 to VPS and bmim; APC-P-75 to bmim; CpTi to VPS and bmim; VPS to APC-CaP -249, and CpTi; bmim to APC-CaP -249, APC-P-75 and CpTi. Screw 'APC-Ca-P-249' showed the greatest cortical thickness, 'bmim' showed the lowest thickness.

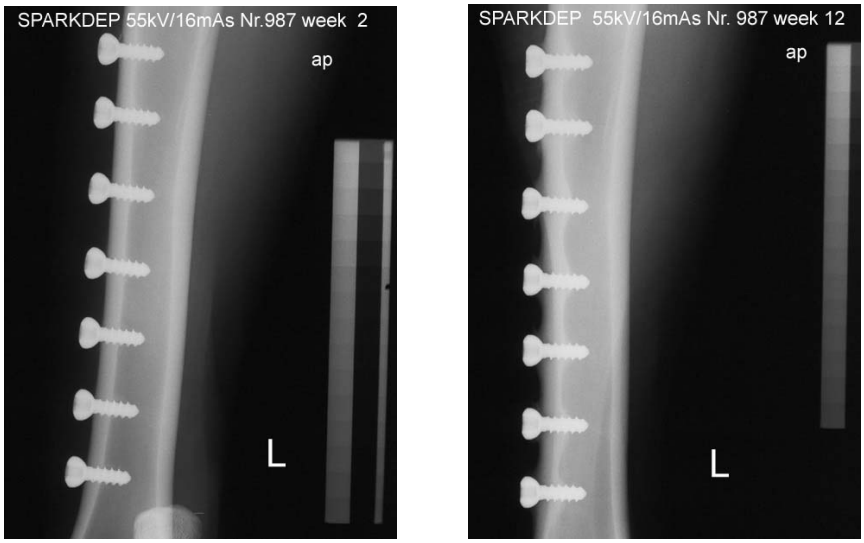

Figure 3.10a X-ray of all screws in left leg at week 2 after surgery showing little *de novo* bone formation at this resolution. b) X-ray of all screws in left leg at week 12 after surgery showing large amounts of *de novo* bone formation on the endosteal side.

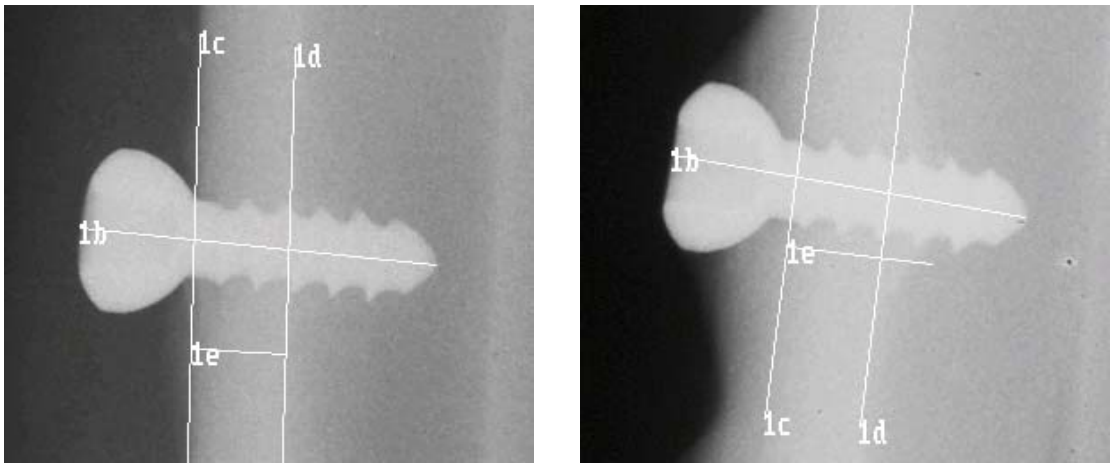

Figure 3.11 The image on the left side shows the length measurement of original cortex at week 2 after surgery (1e). The image on the right side shows the length measurement of original cortex plus callus formation on the endosteal side (1e) ($1e_{right}$ - $1e_{left}$ = length of callus *de novo* bone formation) at week 12 postoperatively.

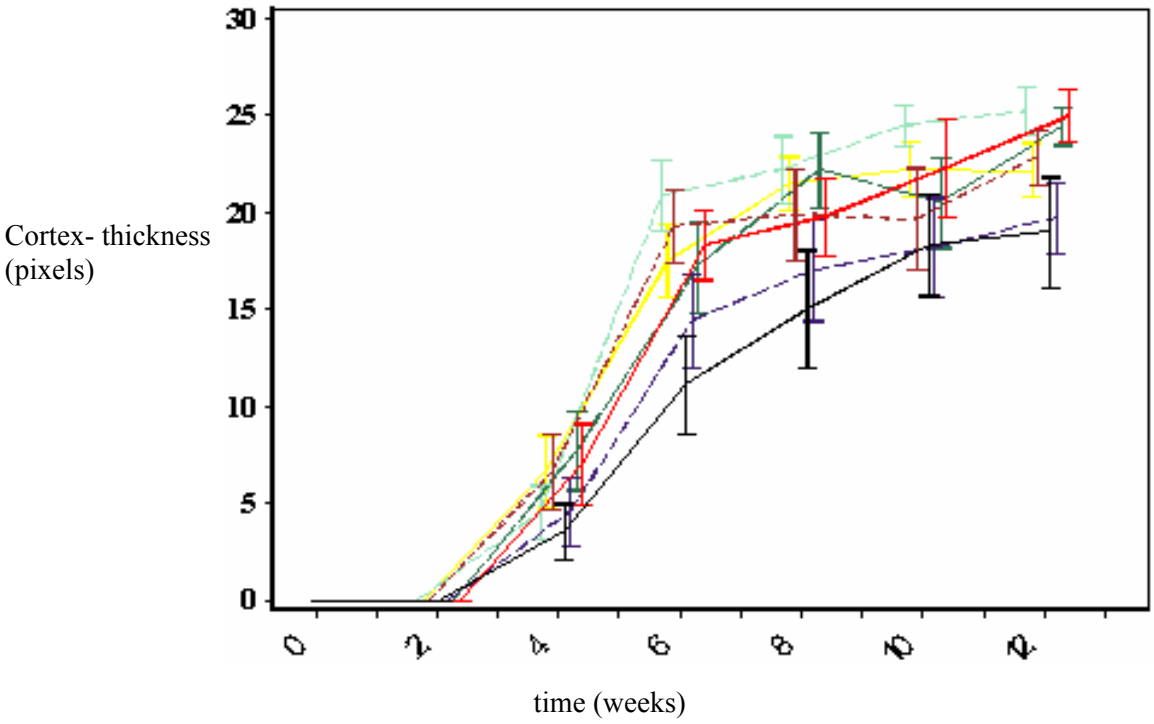

Figure 3.12 Cortical thickening over the 12-week implantation time for all seven screw types. Means +/- SEM. Yellow: APC-P-25, bright green: APC-P-75, red: APC-CaP-249, claret: APC-CaP-360, black: bmim, dark green: CpTi, violet: VPS.

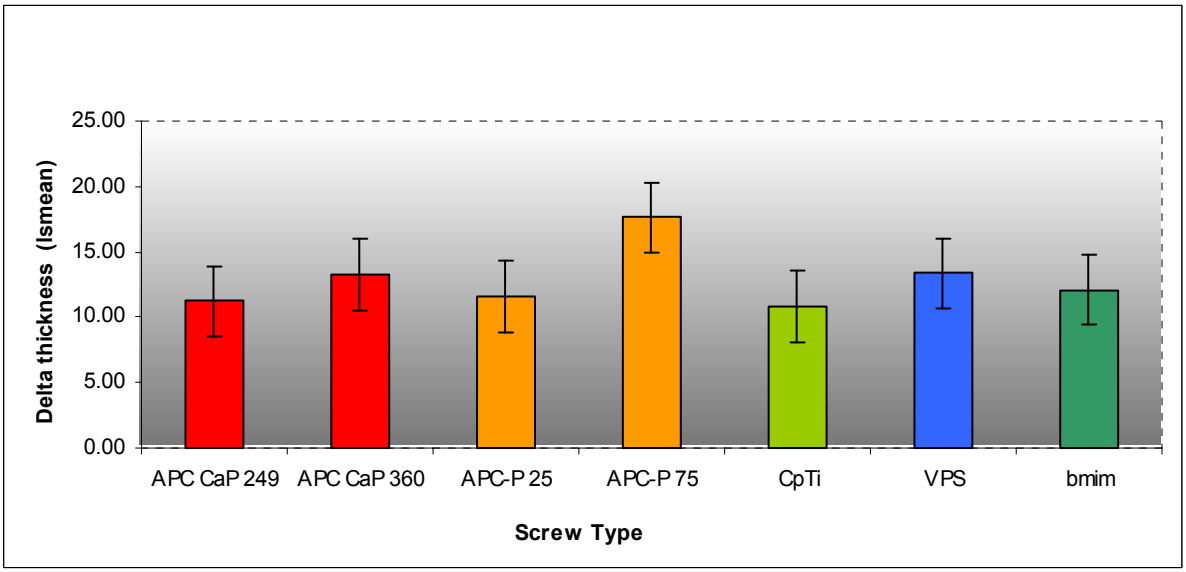

Figure 3.13 Cortical thickness difference observed by radiography between week 4 and 6 post-operation for all seven screw-types. There is no indication for a different bone growth rate between the tested surfaces. The values are least square means adjusted for the animal variations and position of the screw in the tibia by statistical analysis, +/- SEM are shown.

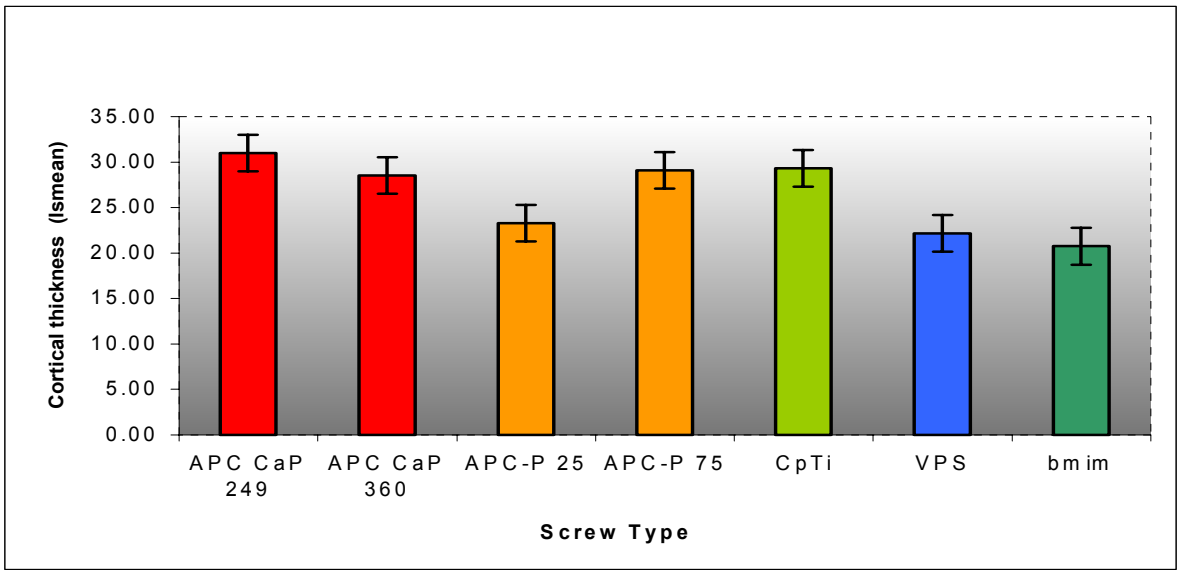

Figure 3.14: Cotical bone thickening observed by radiography at week 12 after implantation for all seven screw-types. The values are least square means adjusted for the animal variations and position of the screw in the tibia by statistical analysis, +/- standard error are shown. The thickness of the cortex of the screw types treated with APC-CaP at the lower current was significantly higher than that of the HA coated screws (VPS and bmim).

Contact radiography

Until week 6 a steep slope of bone formation was detected, followed by a plateau effect. A clear-cut bone enlargement effect was observed in the period of week 2 to week 6 after surgery. During this period of 4 weeks the mean bone formation was 70 % compared to the mean bone formation at week 12 (100%). APC-P-75 showed the largest enlargement rate followed by APC-CaP-360 and VPS, both of which had a similar growth rate to bmim. APC-P-25 and APC-CaP-249 had a similar formation rate. The least rate was with the CpTi (not statistically significant). After week 6 until week 12 a plateau effect was observed. Afterwards, the mean bone formation was only 30 % in the following 6 weeks. Due to this effect one focused only on week 12. The highest thickness was seen with APC-CaP-249, which was statistically significant compared to bmim and VPS followed by CpTi and APC-P-75, which were also significantly higher than bmim and VPS. APC-Ca-P-360 was higher than APC-P-25, bmim and VPS but not statistically significant. Statistically, contact radiography (figure 3.15 and 3.16), compared to the other radiography measurements did not give any extra information, but was required for orientation for sample sectioning.

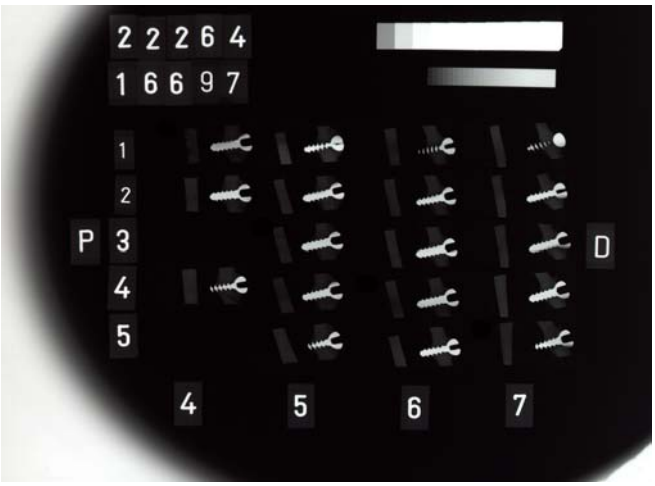

Figure 3.15 Example of a contact radiograp overview exposure. 22264 is the serial exposure number; 16697 is the histological identification number for the sheep; P denotes proximal part of tibia; D denotes distal part of tibia; 4 to 7 (horizontal) denotes the screw number; 1 to 5 (vertical) denotes the section number

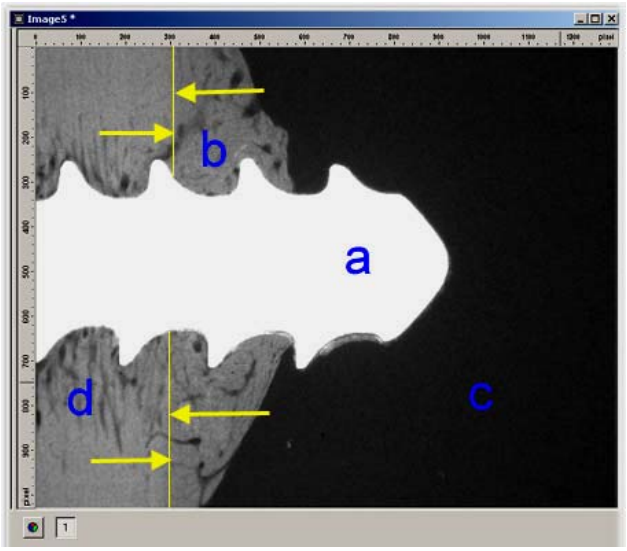

Figure 3.16 Contact radiograph image of a screw tip (a), callus formation (b), medullary canal (c) and original cortex (d) at week 12 post operatively. Yellow arrows mark the border between original bone and newly formed bone.

3.4 Histology

Bright field microscopy

Bone apposition onto the various surfaces of the screws was measured at 12 weeks after histological preparation with bright field microscopy on stained thin sections (figures 3.17-3.20). In the area of the original bone (area of bone remodelling along the drill hole), as well as in the area of the callus formation (area of new bone formation around the tip of the screw in the medullary canal on the endosteal side) no significant differences in the amount of bone formation were observed. Fibrous tissue encapsulating of the implants as well as evidence of neither infection nor loss of bone density associated with any screw was not observed.

The highest screw bone interface-contact values of the calcified fraction of original bone was observed with APC-CaP-360 (64%) and APC-CaP-249 (64%) screw surfaces. All other screw surface types showed the same values (60%). In the area of callus formation (new bone formation around the tip of the screw in the medullary canal on the endosteal side) APC-CaP-

360 showed the highest value (89%) of calcified bone fraction followed by VPS (87%), bmim (86%) and APC-P-75 (85%). The lowest contact was seen with APC-CaP-249 (82%), CpTi (80%) and APC-P-25 (79%). The fraction of calcified bone in contact with the implants for the remodelling of the original cortex is shown in figure 3.21 and similar results in the area of callus formation in figure 3.22.

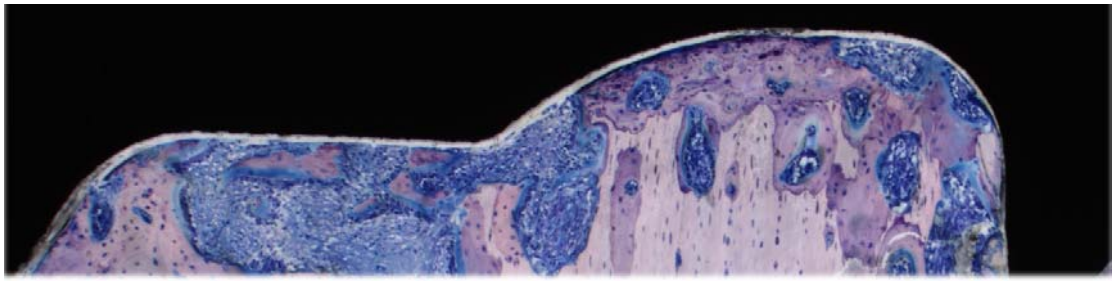

Figure 3.17 Example of the implant bone interface with a lot of gaps filled with soft tissue. The gap between the implant and the tissue is an artefact of histological preparation. (black = section of the implant screw; blue = soft tissue, osteoblasts/ fibroblasts; purple/pink zone = new calcified area- *de novo* bone, light pink zone = original calcified cortical bone).

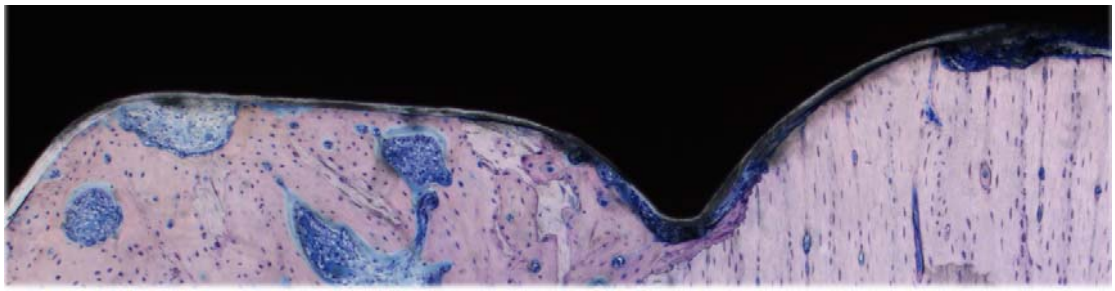

Figure 3.18 Example of the implant bone interface with very few gaps filled with soft tissue (APC-CaP360). The gap between the implant and the tissue is an artefact of histological preparation. (black = section of the implant screw; blue = soft tissue, osteoblasts/ fibroblasts; purple/pink zone = new calcified area- *de novo* bone, light pink zone = original calcified cortical bone)

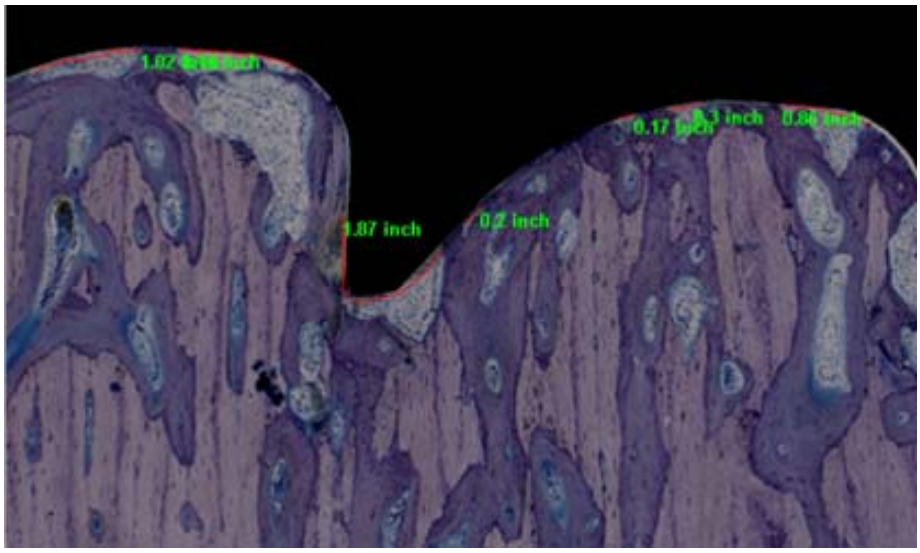

Figure 3.19 Length measurement (red lines) of the gap-zones filled with soft-tissue in the bone remodelling area.

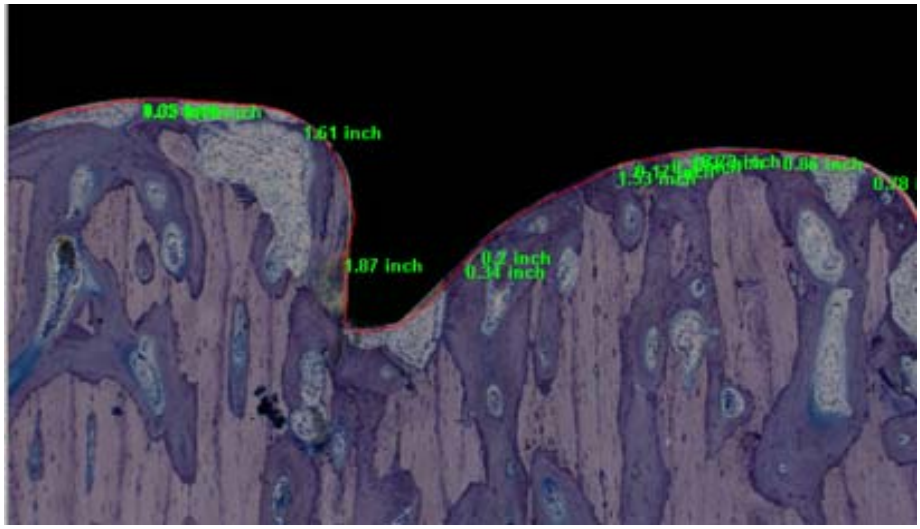

Figure 3.20 Length measurement (red lines) of the gap-zones filled with soft-tissue, plus the bone-implant contact zone in the bone remodelling area.

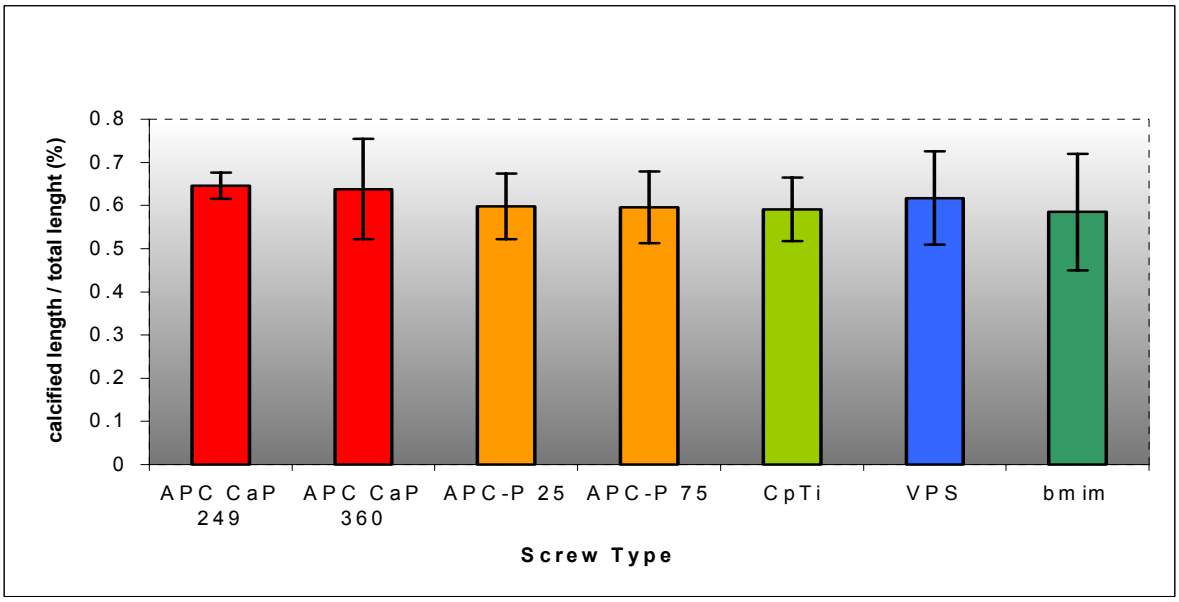

Figure 3.21 Giemsa stained calcified fraction of original bone at week 12 after implantation along the surface contours of the various screw surfaces. There are no significant differences as related to the fraction of calcified interface. The values are least square means adjusted for the animal variations and position of the screw in the tibia by statistical analysis, +/- SEM are shown.

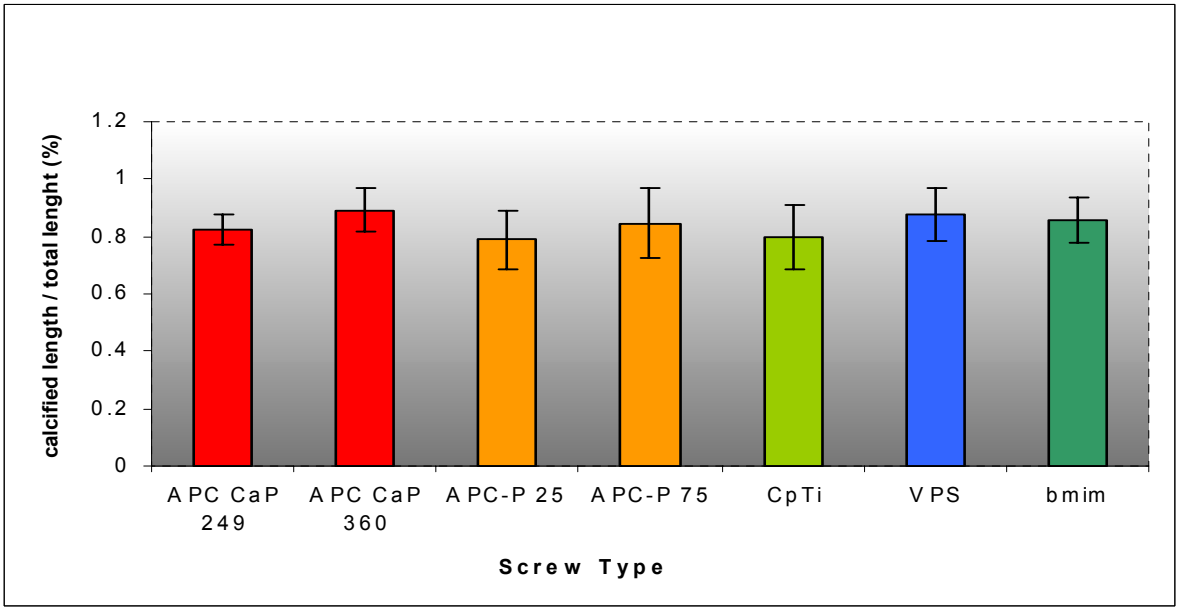

Figure 3.22 Giemsa stained calcified fraction of callus formation (area of new bone formation around the tip of the screw in the medullary canal on the endosteal side) at week 12 after implantation. There are no significant differences as related to the fraction of calcified interface. The values are least square means adjusted for the animal variations and position of the screw in the tibia by statistical analysis, +/- SEM are shown.

Fluorescence microscopy

Fluorescence microscopy showed no difference in magnitude of the rate of bone mineralisation at both the 4 week and 8 week times when the markers were administered (figures 3.23-3.27). Several parts of bone particles on the screw tip, without any connection to the callus formation were not included in the measurement. Those "satellite" bone growth cores were assumed to be related to the drilling process.

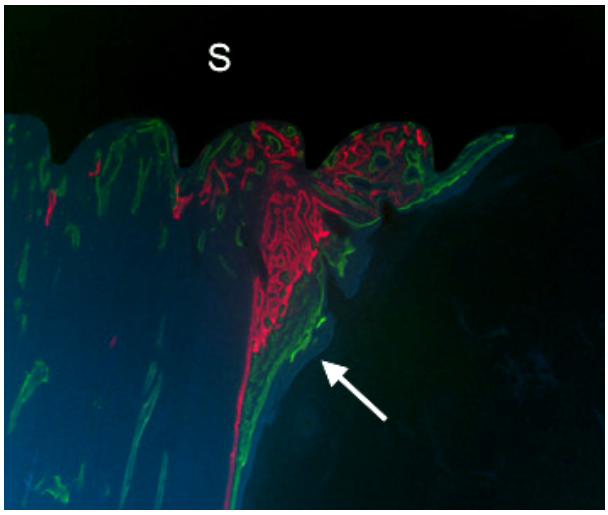

Figure 3.23 Both fluorescent markers of the bone can be seen together in the area of callus formation (with arrow) (red = xylenol orange administered at week 4, green = calcein green administered at week 8). (S) denotes the screw.

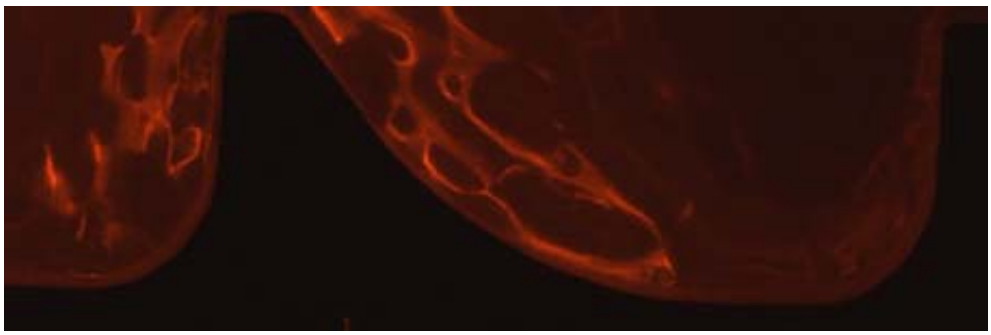

Figure 3.24 Bone sample marked at week 4 post operatively with Xylenol orange. The bright orange areas indicate bone formed at 4 weeks.

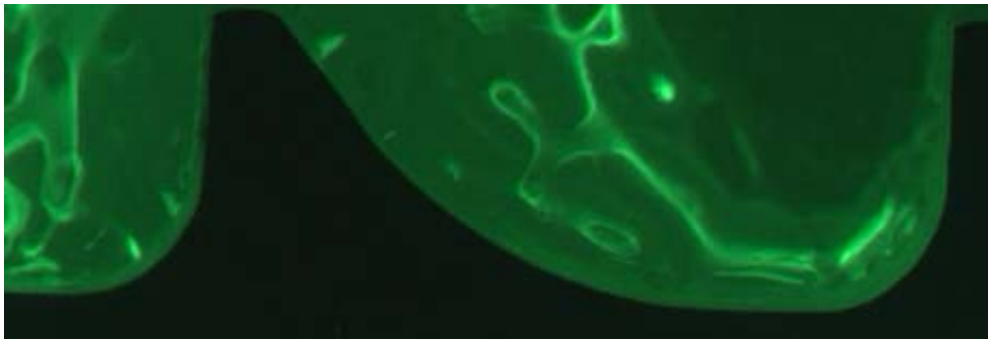

Figure 3.25 Bone sample marked at week 8 post-operatively with Calcein green. The bright green areas indicate bone formed at 8 weeks.

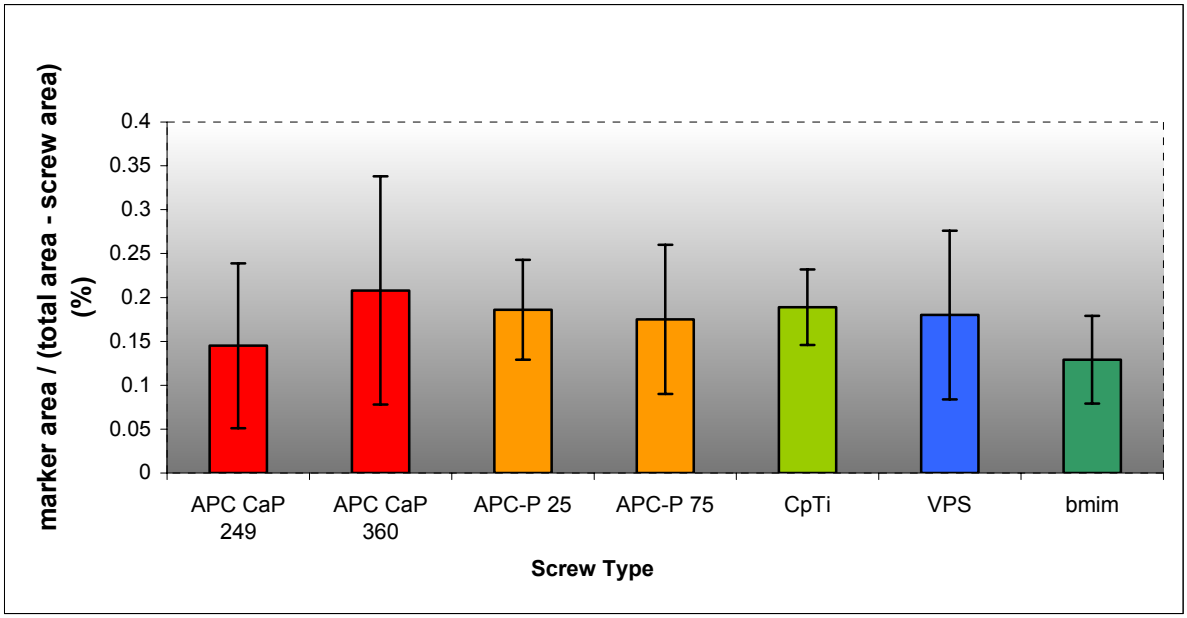

Figure 3.26 Amount of Xylenol orange administered at week 4 observed in fluorescent labelled bone after histological preparation and fluorescence imaging. There are no significant differences in the amount of label between the different surface types. Least square means +/- SEM are shown.

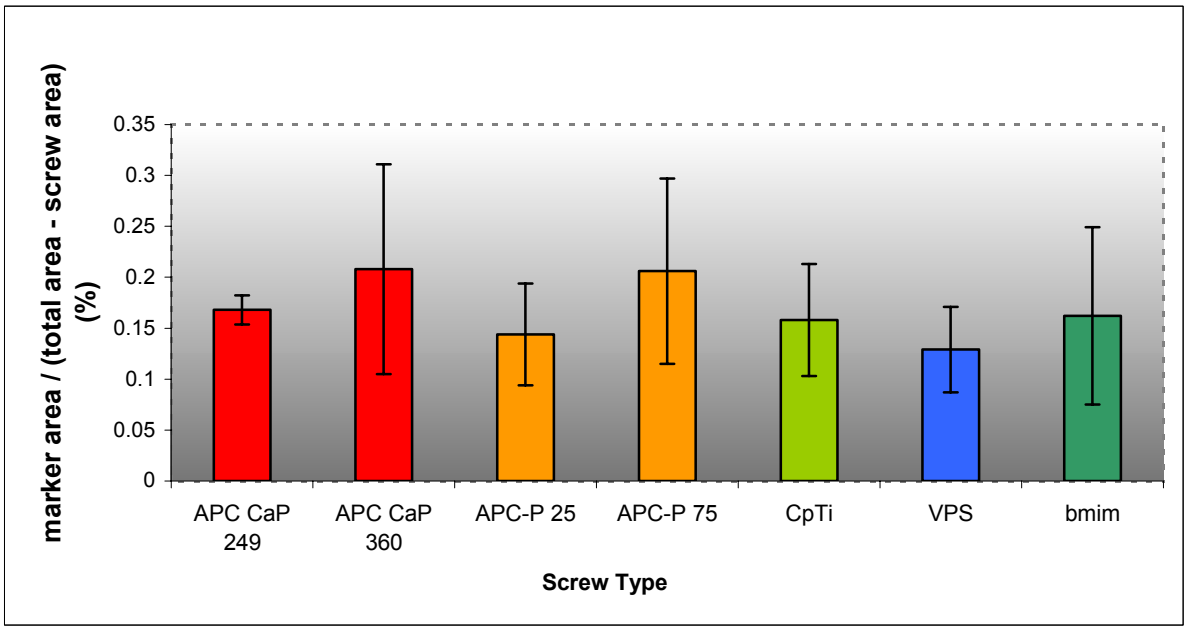

Figure 3.27 Amount of Calcein green administered at week 8 observed in fluorescent labelled bone after histological preparation and fluorescence imaging. There are no significant differences in the amount of label between the different surface types. Least square means +/- SEM are shown.

3.5 Summary of the results

Mechanics

Torque measurements

Tukey and Kramer statistical analysis of the screw insertion torque measurements showed equal torque values at insertion. 14 out of 21 comparisons showed significant differences in screw extraction torque measurements (p-values < 0.05 adjusted by Tukey-Kramer statistics). The extraction effects were much larger than insertion effects, which did not show significant differences for single screws after adjustment though the general screw effect was modestly significant. There was no correlation between insertion torque and extraction torque.

Radiology

In vivo radiology

There was no indication for a different growth rate, from the different surfaces at week 4 and at week 6. At week 12 there were substantial differences: Five out of 21 comparisons showed significant differences with screw 'APC-CaP-249' against 'bmim' showing the greatest difference. There was only a modest effect in growth rate among screw-types between weeks 4 –12. The variability across the time-points was too big to get overall significant differences.

Histology

Bright field microscopy showed no effects upon the calcified area regarding both the remodelling area and the callus area for the various surface types. Fluorescence microscopy of calcein green and xylenol orange labelling showed no significant differences.

4. Discussion

This study assessed the biocompatibility of new anodic plasma chemical treated surfaces when applied to standard titanium screws with regard to both bone remodelling at the surface and *de novo* bone formation within the medullary canal. To verify the implant anchorage in bone several evaluation methods were used which complement each other aimed at reaching an answer on bone formation on the different surfaces during the bone healing process.

Mechanics Torque measurement: To evaluate the implant anchorage, induced by the different surfaces, the focus was placed on the screw extraction torque measurements as Moroni had previously done (Moroni *et al*., 1999). Insertion torque appeared to be lower for VPS, which maybe due to the fracturing of the coating during insertion. These broken parts would remain during the bone remodelling and may help the remodelling, but with their density being similar to bone were not visible in X-Ray imaging.
The VPS and bmim screws showed high extraction torque results, while the APC-CaP-screws showed similar results to the others. The differences observed between the screw types for extraction torque may be attributed to variation between the types of coating thickness, varying from zero on the uncoated titanium (UNT) to 40 µm with the HA coatings (VPS and bmim). The thicker the coating (drill holes having the same size), the higher the preload on the screws, the tighter the fit of the implant in the bone and the better the attachment.

Radiography: The radiography measurements were made *in vivo* over 12 weeks using 7 time points. Information about the bone growth rate over a time window with clinical relevance was obtained as well the total amount of bone formed at the end of the experiment. There is a clear trend that the irregular-rough APC coated surfaces initially induced good bone forming activity observed until week 6. Similar activity was observed with VPS. In the study of Moroni only two time points were used, one at surgery and one at euthanasia (Moroni *et al*. 1999). Due to this the answer was just that bone growth and cortex thickening were observed and there were no results on initial growth rate. Fini *et al*. (1999) only used histomorphometric analysis and microradiographic evaluation and therefore were also not able to state what happened over time with the bone growth.

Histology

Bright field microscopy: The zone without remodelling within the cortex was not addressed in this evaluation, nor was the new bone grown around the screw head. There was inconsistency in coating of the head from the suppliers, which could not be changed in time for surgery (screw heads of VPS screws were not coated, bmim ones partially coated, while APC treated screws were fully coated during production). The zone of remodelling at week 4 and at week 8 was still influenced by trauma of the drilling process during the operation. This effect seemed to have had more impact on bone remodelling than the surface of the screws. Thus it would not be realistic to give an answer about biocompatibility of the screw surface in this area at these time points. For the quantitative comparison of Giemsa stained sections the remodelling zone was used, since the evaluation was conducted at week 12. At this later stage of the healing process the effect of destroying the bone tissue during drilling was thought to have less influence than the different screw surfaces on bone remodelling. The new *de novo* bone growth zone around the screw tip was important for the Giemsa stained sections as well as for the fluorescent marked sections. The reason why this area was so important was that only new bone, without remodelling of old bone from the drilling process was observed. The surface of the screw was therefore thought to be the most important factor for *de novo* bone growth in this area. Thus it gave a comparable opinion on biocompatibility of the screw surfaces in this area.

Bone Contact relation to Torque measurements: Moroni *et al*., (1999) explained the high extraction torque measurements found in their study for the fluoro-hydroxyapatite coated screws, as being due to the extensive close and direct bone contact found in their histological evaluation of this coating. For the VPS (HA plasma coated) screws we have found the same correlating results between extraction torque and histomorphometric results as Moroni showed. The APC-CaP screws showed significantly lower extraction torque values compared to VPS, and surprisingly more calcified screw to bone contact in the old bone area. Our results did not show any correlations between the bone bonding strength, measured by the extraction torque, and the quality of the bone surrounding the screws. This was in contrary to the results of Moroni *et al*. (1999). It seems that new parameters have to be included in the screw-series, such as coating thickness and bonding strength of the coatings to the implant surface as related to the extraction torque. If one focuses on the coating thickness, it can be seen that the thickness differs between 2 μm and 40 μm and the highest extraction torque measurement results were obtained for the screws with the thickest coating.

Fluorescence microscopy: Fluorescent markers were used for identification of newly formed bone, determination of amount of bone formed, direction and time of bone deposition, bone remodelling and mineralisation processes. Fluorescent substances, which form chelate complexes with apatite were administrated at predetermined times. The sequential use of labelling substances of different colours allowed easier identification and better analysis of changes with time. Fluorescent substances can be detected at low concentrations, which are non-toxic. All these substances required undecalcified processing for histology, since they are bound to the mineral phase of bone. In the area of the callus formation, the amount of bone growth observed by measuring the amount of labelled bone did not show significant differences. This was the case for week 4 (xylenol orange) and week 8 (calcein green). The variation was too large to produce any ranking order of bone formation at these times.

Problems during in vivo experiments: Two sheep died at surgery. This was due to several factors: Anaesthesia: Halothane was used without spinal anaesthesia. A high halothane flow, with non-relaxed legs may have been the main problem. This may have induced a dangerous shock situation (pathological report, Veterinärmedizinische Fakultät, University of Zürich). As a consequence, the anaesthesia management was changed for all sheep (see materials and methods: Anaesthesia) in this study. The postoperative healing process showed no problems in seven sheep. One sheep developed an infection on the right tibia. With intensive wound care it was possible to manage the infection without antibiotics, but the affected tibia was excluded from the study.

Regarding the biocompatibility of the APC surfaces, the early bone induction and the amount of calcified bone implant contact of the modified APC surface was as good as for the known HA surfaces. In addition results from L.C. Baxter (Baxter *et al*. 2002) showed that the APC-CaP and produce a greater amount of spreading with osteoblasts and fibroblasts, and adhesion in fibroblasts (osteoblasts were not tested) *in vitro*, than the APC-P and bmim samples tested. VPS samples were not tested in the *in vitro* study. A follow up study with loaded implants was also performed at the AO Research Institute with the APC-CaP coating and the abstract (presented at the 2003 ORS- Orthopaedic Research Society meeting) can be seen in the appendix.

5. Conclusions

The findings of the present investigation demonstrated that the screws coated with the APC method proved to be biocompatible for both bone remodelling at the surface and *de novo* bone formation. Regarding the bone growth induction and apposition onto the implant surfaces, the APC treated screws behaved as well as both commercial HA coatings (VPS and bmim). The uncoated titanium screws (UNT) showed the lowest bone apposition at this stage (but having no coating had no pre-load for bone apposition). However, the anchorage of the HA coatings were stronger than the APC coatings, but this is very likely to be due to the influence of the coating thickness on the pre-load and therefore anchorage of the implants. The non-loaded model with screws does not appear to be sensitive enough to show differences that may occur in clinical situations with other types of implants (e.g. spine cage). If a steel screw was used as a (less biocompatible) control, a difference may have been observed.

Furthermore, the mechanical properties of the APC coatings are clearly superior to the HA coatings (VPS and bmim). The APC screws showed superior bonding strength to the implant surface in comparison to plasma sprayed and chemically prepared HA (performed according to ISO 13779-4) (Frauchiger, PhD thesis). The APC coating method would appear to have many advantages over HA coatings and is as biocompatible. The higher implant-bonding strength of APC coatings compared to HA would suggest use for pins for fracture fixation and since it can be used to coat any three-dimensional shape could have huge potential for implants such as spine cages.

6. References

Albrektsson T, Branemark PI, Hansson HA, Lindstrom J (1981) Osseointegrated titanium implants. Requirements for ensuring a long-lasting, direct bone-to-implant anchorage in 410 man. *Acta Orthop.Scand.* 52:155-170

Albrektsson T, Johansson C (2001) Osteoinduction, osteoconduction and osseointegration. *Eur.Spine J.* 10 Suppl 2: S96-101

Bagambisa FB, Joos U (1990). Preliminary studies on the phenomenological behaviour of osteoblasts cultured on hydroxyapatite ceramics. *Biomaterials* 11, 50-56.

Baxter LC, Frauchiger V, Textor M, Gwynn I, Richards RG (2002). Fibroblast and osteoblast adhesion and morphology on calcium phosphate surfaces. *Eur Cell Mater* 4, 1-17.

Branemark PI, Hansson BO, Adell R, Breine U, Lindstrom J, Hallen O, Ohman A (1977). Osseointegrated implants in the treatment of the edentulous jaw. Experience from a 10- 420 year period. *Scand.J.Plast.Reconstr.Surg.Suppl;* 16:1-132

Buser D, Schenk RK, Steinemann S, Fiorellini JP, Fox CH, Stich H (1991). Influence of surface characteristics on bone integration of titanium implants. A histomorphometric study in minature pigs. *J.Biomed.Mat.Res.* 25, 889-902.

Chae JC, Collier JP, Mayer MB, Surprenant VA, Dauphinais LA (1992). Enhanced ingrowth of porous coated CoCr implants plasma spray with tricalcium phosphate. *J. Biomed. Mat. Res.* 56, 93-102.

Davies JE (1998). Mechanisms of endosseous integration. *International J. Prosthodontics* 11 (5), 391-401.

Ducheyne P, Qiu Q (1999) Bioactive ceramics: the effect of surface reactivity on bone formation and bone cell function. *Biomaterials* 20: 2287-2303

Fini M (1999). *In vitro* and *in vivo* behaviour of Ca and P enriched anodized titanium. *Biomaterials* 20 (17), 1587-1594

Frauchiger VM (2002). Anodic Plasma-Chemical Treatment of Titanium Implant Surfaces. *Thesis: Department of Materials ETH Zürich* 14720

Gemmell CH. & Park, JY. (2000). Initial Blood interactions with endosseous implant materials. In "Bone Engineering" editor J.E. Davies. em squared inc. Toronto. pp.108-117.

Gruner H (2001). Thermal spray coatings on titanium. In Brunette DM, Tengvall P, Textor M, Thomsen P, eds. Titanium in Medicine. Berlin & Heidelberg:Springer-verlag, 375-416.

Hanawa T, Kamiura Y, Yamamoto S, Kohgo T, Amemiya A, Ukai H, Murakami K, Asaoka K (1997) Early bone formation around calcium-ion-implanted titanium inserted into rat tibia. *J. Biomed Mater Res* 36, 131-136.

Ishizawa H, Fujino M, Oginio M (1995). Mechanical and histological investigation of hydrothermally treated and untreated anodic titanium-oxide films containing Ca and P. *J. Biomed. Mat. Res.* 29, 1459-1468

Ishizawa H, Fujino M, Oginio M (1997). Histomorphometric evaluation of the thin hydroxyapatite layer formed through anodisation followed by hydrothermal treatment. *J. Biomed. Mat. Res.* 35, 199-206

Ishizawa H, Oginio M (1995). Characterisation of thin hydroxyapatite layers formed on anodic titanium-oxide filmes containing Ca and P by hydrothermal treatment. *J. Biomed. Mat. Res.* 29, 1071-1079

Ishizawa H, Oginio M (1995). M. Formation and characterisation of anodic titanium oxide films containing Ca and P. *J. Biomed. Mat. Res.* 29, 65-72

Kim HM, Miyaji F, Kokubo T, Nishiguchi S, Nakamura T (1999). Graded surface structure of bioactive titanium prepared by chemical treatment. *J. Biome Mat Res*, 45 (2) 100-107.

Kurze P, Knofler W (1986). Anodic oxidation under spark discharge (ANOF) – a new coating procedure in medical technology. *J. Klinische Medizin-ZKM* 41 (3), 219-222

Lausmaa J, Radegran D (1991). Preparation of ultra-thin oxide windows on titanium for tem analysis. *J. Electron Microscopy Technique* 19 (1), 99-106

Moroni A, Caja V, Sabato C, Egger EL, Gottsauner-Wolf F, Chao EYS (1994). Bone ingrowth analysis and interface evaluation of hydroxyapatite coated versus uncoated titanium porous bone implants. *J.Mat.Sci.Mat.Med* 5, 411-416.

Moroni A, Orienti L, Stea S, Visentin M (1996). Improvement of the bone-pin interface with hydroxyapatite coating: an *in vivo* long-term experimental study. *J.Orthop.Trauma* 10, 236-242

Moroni A, Faldini C (1999). The effect of surface material and roughness on bone screw stability. *J. Orthop. Trauma* 13 (7), 477-482

Nygren H, Eriksson C, Lausmaa J (1997). Adhesion and activation of platelets and polymorphonuclear granulocyte cells at TiO2 surfaces. *J. Laboratory and Clinical Medicine* 129 (1), 35-46

Osborn, JF. and Newesley, H. (1980). Dynamics aspects of the implant-bone interface. In Heimke, G. (ed). Dental Implants- Materials and Systems.Munich: Carl Hanser, 111-123.

Park JY, Gemmelll CH, Davies JE (2001). Platelet interactions with titanium: modulation of platelet activity by surface topography. *Biomaterials* 22 (19), 2671-2682

Pommer A, Muhr G, David A (2002). Hydroxyapatite-coated Schanz pins in external fixators used for distraction osteogenesis : a randomized, controlled trial. *J.Bone Joint Surg.Am.* 84-A, 1162-1166.

Rahn BA, Perren SM (1971). Xylenolorange, a fluorochrome useful in polychrome sequential labelling of calcifying tissues. *Stain Technol* 46,125-129

Richards RG, ap Gwynn I. (1995). Backscattered electron imaging of the undersurface of resin-embedded cells by field-emission scanning electron microscopy. *J. Microsc.* 177: 43-52.

Richards RG, Stiffanic M, Owen GRh, Riehle M, ap Gwynn I Curtis ASG. (2001). Immunogold labelling of fibroblast focal adhesion sites visualised in fixed material using scanning electron microscopy, and living, using internal refection microscopy. *Cell Biol. Int.* 25 (12): 1237-1249

Rokkum M, Reigstad A, Johansson CB, Albrektsson T (2003). Tissue reactions adjacent to well-fixed hydroxyapatite-coated acetabular cups. Histopathology of ten specimens retrieved at reoperation after 0.3 to 5.8 years. *J.Bone Joint Surg.Br.* 85, 440-447

Schreckenbach J, Schlottig F, Marx G (1999). Preparation and characterisation of chromium and sodium tantalate layers by anodic spark deposition. *J. Analytical Chemistry* 363 (2), 209-211

Schreckenbach J, Schlottig F, Marx G (1999). Preparation and microstructure characterization of anodic spark deposited barium titanate conversion layers. *J. Materials Research* 14 (4), 1437-1443

Schreckenbach J, Schlottig F, Marx G, Textor M, Spencer ND (1999). Characterization of anodic spark-converted titanium surfaces for biomedical applications. *J. Mat.Sci.Mat.Med* 10 (8), 453-457

Searle SR, Speed FM, Milliken GA (1980). Population marginal means in the linear model: an alternative to the least squares means. *The American Statistician* 34, 216-221

Shen X (1993). Organic extracellular-matrix components at the bone cell-substratum interface. *Cells & Materials* 3 (3), 257-272

Suzuki HK, Mathews A (1966). Two colour fluorescent labelling of mineralizing tissues with tetracycline and 2,4-bis(N,N'-di(carbomethyl)aminomethyl) fluorescein. *Stain Technol* 41:57-60

Witt M, Kulisch W (1991). Characterization of remote plasma enhanced chemical vapor-deposition process. *Material Science and Engineering A-Structural Materials Properties Microstructure and Processing* 140, 715-721

7. Acknowledgements

I would like to thank the following people for their help during the duration of my thesis and my time in Davos. First I would like to thank my supervisors Dr. R.G. Richards and Prof. Dr. med. vet. J. Auer for guidance.
I would also like to thank Prof. Dr. sc. techn. E. Schneider for allowing me to perform this work at the AO Research Institute in Davos.

I would like to thank all those at the AO Research Institute in Davos for being lovely people to work with. Specifically I would like to thank and acknowledge:

Dr. Geoff Richards for all his good advice and enthusiastic help during my work plus performing SEM and laser profilometry imaging of screws, and for his help with thesis writing.
Prof. Dr. Berton Rahn - teaching in light microscopy, using image analysis programs and giving specific histological advice and also for his help with my manuscript.
Ronald Wieling - teaching me practical surgery and giving advice in this area.
The animal care team – helping to look after the sheep.
Dr. Vinzenz Frauchiger – producing the plasma-chemically treated samples, carrying out the XPS measurements and his help with the histological evaluation.
Dr. Dominik Pfluger and Dr. Keita Ito – helping with statistical calculations.
Stratec Medical, Dr. Robert Mathys Foundation (RMS), AO-Research Institute for funding the project.(KTI/Med Tech Grant no. 4729).
Dr. Falco Schlottig (Stratec Medical).
Dr. Beat Gasser (RMS) for implant materials and helpful discussions.

I feel that special mention should go to the members of the Interface Biology Group, Histology Group, the Anaesthesia Team and the members of the Research Service (specially: Oli Bösl, Dieter Wahl and Berend Linke).

I would like to thank my family and my girlfriend for supporting me emotionally through this thesis.

8. Appendix

Contact radiography (KS 400-macro):

```
imgdelete "*"
Gclear 0

#  Kalibrierung laden (micrometer/pixel)
MSsetgeom

imgsetpath "f:\"
! imgload "image.tif",1
imgdisplay 1

! Grectg 166,232,900,900,15,7
Gmerge 2,255
binand 2,1,3
dislev 3,4,228,255,1
bindilate 4,4,6,1
imgdisplay 4
Gclear 0

MSmeasmask 4,4,"DATABASE",0,1,10
MSdrawmask 4,4
datalist "DATABASE",0,1
pause "Daten in Excel pasten nicht vergessen !!!",0

dislev 4,5,255,203,1
binand 5,3,6
imgdisplay 6
Gclear 0
! dislev 6,7,75,255,1
imgdisplay 7
Gclear 0
MSmeasmask 7,7,"DATABASE",0,1,10
MSdrawmask 7,7
datalist "DATABASE",0,1
pause "Daten in Excel pasten nicht vergessen !!!",0

dislev 7,8,255,72,1
binand 8,2,9
binand 9,5,9
imgdisplay 9
Gclear 0
MSmeasmask 9,9,"DATABASE",0,1,10
MSdrawmask 9,9
datalist "DATABASE",0,1
pause “Daten in Excel pasten nicht vergessen !!!“
```

Fluorescence microscopy (KS 400-macro):

```
imgdelete "*"
Gclear 0
MSsetgeom

! imgload "d:\patrick schlegel\*.tif",1
imgdisplay 1
! dislev 1,2,0,13,1
binscrap 2,3,0,5,0
!bindilate 3,4,7,1
showwindow "editor",1
imgdisplay 4
!binclose 4,4,6,1
MBok "beim nächsten treshold Schneeflocken entfernen"
!dislev 4,4,240,255,1
!MSmeasmask 4,4,"DATABASE",0,1,10
datalist "DATABASE",0,1
pause "Daten in Excel pasten",0
imgcopy 1,5
Gclear 0
imgdisplay 5
! dislev 5,6,39,255,1
MSsetgeom
MSmeasmask 6,6,"DATABASE",0,1,10
datalist "DATABASE",0,1
pause "Daten in Excel pasten",0
dislev 6,7,153,189,1
dislev 7,80,36,1
MSmeasmask 80,80,"DATABASE",0,1,10
datalist "DATABASE",0,1
pause "Daten in Excel pasten",0
```

Raw data Torque measurements after taking averages.

Obs	ANIMAL	SIDE	POSSCREW	TORQ_IN	TORQ_ex
1	74	L 1	APC-P-75	0.0984	0.5663
2	74	L 2	bmim	0.0982	0.7507
3	74	L 3	VPS	0.0804	0.8798
4	74	L 4	UNT	0.0722	0.6288
5	74	L 5	APC-CaP-249	0.1936	0.6771
6	74	L 6	APC-CaP-360	0.1228	0.6925
7	74	L 7	APC-P-25	0.0764	0.6436
8	121	L 1	APC-P-25	0.0866	0.6561
9	121	L 2	APC-P-75	0.0706	0.6744
10	121	L 3	bmim	0.1080	0.7825
11	121	L 4	VPS	0.0819	0.8252
12	121	L 5	UNT	0.0849	0.6165
13	121	L 6	APC-CaP-249	0.1391	0.6588
14	121	L 7	APC-CaP-360	0.1385	0.6212
15	135	L 1	APC-CaP-249	0.1190	0.6262
16	135	L 2	APC-CaP-360	0.1236	0.6296
17	135	L 3	APC-P-25	0.1117	0.6241
18	135	L 4	APC-P-75	0.1310	0.4151
19	135	L 5	bmim	0.1343	0.7259
20	135	L 6	VPS	0.0792	0.7612
21	135	L 7	UNT	0.0777	0.5436
22	945	L 1	UNT	0.0695	0.5692
23	945	L 2	APC-CaP-249	0.0532	0.6386
24	945	L 3	APC-CaP-360	0.0884	0.6372
25	945	L 4	APC-P-25	0.1506	0.7605
26	945	L 5	APC-P-75	0.0607	0.6360
27	945	L 6	bmim	0.1656	0.7091
28	945	L 7	VPS	0.0481	0.7897
29	968	L 1	bmim	0.1295	0.7750
30	968	L 2	VPS	0.0700	0.6040
31	968	L 3	UNT	0.0710	0.5895
32	968	L 4	APC-CaP-249	0.0996	0.7161
33	968	L 5	APC-CaP-360	0.0978	0.7413
34	968	L 6	APC-P-25	0.0682	0.6399
35	968	L 7	APC-P-75	0.0692	0.6519
36	980	L 1	APC-CaP-360	0.0934	0.4151
37	980	L 2	APC-P-25	0.0736	0.5872
38	980	L 3	APC-P-75	0.0701	0.5835
39	980	L 4	bmim	0.0930	0.7011
40	980	L 5	VPS	0.0670	0.7714
41	980	L 6	UNT	0.0726	0.5130
42	980	L 7	APC-CaP-249	0.0704	0.5875
43	983	L 1	VPS	0.0758	0.8587
44	983	L 2	UNT	0.0904	0.6253
45	983	L 3	APC-CaP-249	0.1077	0.6886
46	983	L 4	APC-CaP-360	0.0952	0.7141
47	983	L 5	APC-P-25	0.0864	0.6353
48	983	L 6	APC-P-75	0.0820	0.5880
49	983	L 7	bmim	0.0761	0.7040
50	987	L 1	bmim	0.0523	0.7665
51	987	L 2	VPS	0.0784	0.8819
52	987	L 3	UNT	0.1146	0.6301
53	987	L 4	APC-CaP-249	0.0795	0.6807
54	987	L 5	APC-CaP-360	0.1062	0.6803
55	987	L 6	APC-P-25	0.0764	0.6452
56	987	L 7	APC-P-75	0.0733	0.6452

Raw-data: Calcified fraction (calcified length/total)

			Re-modelling		Callus area		fractions	
animal	**pos**	**screw**	**calc1**	**gap1**	**calc2**	**gap2**	**tot1**	**tot2**
16635/74	1	APC-P-75	31,7	21,81	18,94	7,57	53,51	26,51
16635/74	2	Bmim	25,26	21,6	26,81	10,32	46,86	37,13
16635/74	3	VPS	18,77	22,37	33,61	8,45	41,14	42,06
16635/74	4	UNT	17,81	21,03	19,36	0,72	38,84	20,08
16635/74	5	APC-CaP-249	32,21	20,13	11,3	1,29	52,34	12,59
16635/74	6	APC-CaP-360	24,55	10,75	20,91	1,03	35,3	21,94
16635/74	7	APC-P-25	23,92	11,68	13,17	0,58	35,6	13,75
16636/121	1	APC-P-25	25,4	21,36	17,07	6,46	46,76	23,53
16636/121	2	APC-P-75	26,85	14,98	22,93	6,42	41,83	29,35
16636/121	3	bmim	26,33	14,59	19,86	1,43	40,92	21,29
16636/121	4	VPS	23,6	9,93	22,42	5,04	33,53	27,46
16636/121	5	UNT	19,72	11,41	19,99	8,27	31,13	28,26
16636/121	6	APC-CaP-249	24,93	13,89	18,32	4,72	38,82	23,04
16636/121	7	APC-CaP-360	27,66	5,73	12,74	2,59	33,39	15,33
16689/983	1	VPS	37,8	13,75	25,55	1,15	51,55	26,7
16689/983	2	UNT	29,74	13,63	18,02	3,06	43,37	21,08
16689/983	3	APC-CaP-249	26,65	14,72	15,94	2,84	41,37	18,78
16689/983	4	APC-CaP-360	25,56	13,84	22,91	0,86	39,4	23,77
16689/983	5	APC-P-25	20,87	11,76	13,1	5,45	32,63	18,55
16689/983	6	APC-P-75	21,25	10,37	10,63	5,15	31,62	15,78
16689/983	7	bmim	18,79	10,7	14,47	1,64	29,49	16,11
16690/135	1	APC-CaP-249	25,05	14,3	21,18	3,94	39,35	25,12
16690/135	2	APC-CaP-360	32,49	14,74	17,17	5,06	47,23	22,23
16690/135	3	APC-P-25	24,19	12,02	25,67	13,7	36,21	39,37
16690/135	4	APC-P-75	23,2	14,11	17,87	2,3	37,31	20,17
16690/135	5	bmim	27,38	7,83	19,1	2,69	35,21	21,79
16690/135	6	VPS	7,27	7,08	11,9	0	14,35	11,9
16690/135	7	UNT	14,97	8,23	14	2,87	23,2	16,87
16691/945	1	UNT	22,23	15,83	15,94	6,73	38,06	22,67
16691/945	2	APC-CaP-249	29,18	18,38	11,6	2,24	47,56	13,84
16691/945	3	APC-CaP-360	26,86	17,69	20,73	3,48	44,55	24,21
16691/945	4	APC-P-25	25,6	24,6	17,83	3,2	50,2	21,03
16691/945	5	APC-P-75	17,03	23,12	23,1	1,62	40,15	24,72
16691/945	6	bmim	30,22	16,09	10,68	1,13	46,31	11,81
16691/945	7	VPS	23,34	9,16	14,59	4,06	32,5	18,65
16696/968	1	bmim	17,75	30,26	20,36	2,59	48,01	22,95
16696/968	2	VPS	26,58	18,73	17,41	0,84	45,31	18,25
16696/968	3	UNT	24,63	20,15	23,01	3,24	44,78	26,25
16696/968	4	APC-CaP-249	31,8	13,91	9,05	3,24	45,71	12,29
16696/968	5	APC-CaP-360	17,93	18,52	18,99	1,36	36,45	20,35
16696/968	6	APC-P-25	17,31	17,04	14,05	3,57	34,35	17,62
16696/968	7	APC-P-75	17,53	13,27	17,31	0,9	30,8	18,21
16697/987	1	bmim	19,48	21,65	28,89	8,09	41,13	36,98
16697/987	2	VPS	26,02	16,39	19,49	4,4	42,41	23,89
16697/987	3	UNT	25,89	18,93	29,11	14,99	44,82	44,1
16697/987	4	APC-CaP-249	33,09	15,85	18,97	4,74	48,94	23,71
16697/987	5	APC-CaP-360	15,14	14,38	23,98	1,43	29,52	25,41
16697/987	6	APC-P-25	24,41	13,2	14,63	2,85	37,61	17,48
16697/987	7	APC-P-75	16,74	9,12	20,72	0,39	25,86	21,11

CURRICULUM VITAE

Name/Vorname: med.vet. Patrick Schlegel

Wohnsitz: 9470 Buchs, Montfortweg 10
Geburtsdatum: 26. März 1974
Nationalität: CH
Zivilstand: ledig

AUSBILDUNG / QULAIFIKATIONEN:

Seit 2002	Kleintierklinik-ACR in Winterthur (Assistent)
2001/2003	AO-Forschungsinstitute Davos (Dissertation)
1994-2000	Veterinärmedizinische Fakultät Universität ZH Abschluss: Diplom, November 2000
1989-1994	Matura Typus C an der Kantonsschule Sargans Abschluss: Diplom, Januar 1994
1987/1988	Sekundarschule: 9470 Buchs

WEITERBILDUNGEN / PRAKTIKA

Weiterbildungen und Praktika an den Veterinärmedizinischen Fakultäten der Universitäten Zürich und Bern sowie am AO-Forschungsinstitut Davos
(Zoo - u. Heimtiere, Kleintierchirurgie, AO - Course-2001, Hämatologie Flims 2004)